MOLECULAR INDICATORS FOR THE SEVERITY OF SINDBIS VIRUS-INDUCED ENCEPHALOMYELITIS

by

KUO GAI

A THESIS SUBMITTED TO JOHNS HOPKINS UNIVERSITY IN CONFORMITY WITH THE REQUIREMENTS FOR THE DEGREE OF MASTER OF SCIENCE

BALTIMORE, MARYLAND

MAY, 2017

Abstract

The alphavirus Sindbis virus (SINV) serves as a model for studying the mechanisms of viral encephalomyelitis. Severity of SINV diseases is determined by multiple factors including the host immune response and virus strain. Neuroadapted Sindbis virus (NSV) causes severe encephalomyelitis with prominent hindlimb paralysis. Toll-like receptors (TLRs) are major regulators of antiviral responses, but may also trigger innate immunity-mediated damage to neurons. Endosomal TLR stimulation by pathogen/ damage-associated molecular patterns (PAMPs or DAMPs) such as misregulated microRNAs can directly cause neuronal cell death. Previous microarray analysis has identified two upregulated miRNAs during SINV infection in mice. As a result, the first goal of this study was to evaluate the regulation of endosomal TLRs, associated adaptors and the two deregulated miRNAs in SINV-infected mice. We also explored the hypothesis that necroptosis, a newly described regulated necrosis pathway, contributes to motor neuron degeneration within the spinal cord following infection with NSV strain of SINV. This proinflammatory mode of cell death could potentially result in direct neuronal death and amplify neuroinflammation that reflects the severity of SINV-induced encephalomyelitis.

Acknowledgments

Firstly, I would like to express my sincere gratitude to my advisor, Dr. Diane Griffin for providing me the opportunity to conduct research in her laboratory, and also for her continuous support and guidance during my study. I would also like to thank Dr. Victoria Baxter who served as my mentor when I first joined the lab and taught me majority of the experimental skills involved in this project. She was always patient whenever I have any questions and also gave me advice about data analysis, interpretation and presentations. Besides, I would like to thank other members of Griffin Lab. Jane Xie helped me greatly with me western blotting and related assays. I am also grateful to Elizabeth Troisi and Nina Martin for their help with the immunohistochemistry protocol and other experiements. Debbie Hauer kindly support my work when I need ant reagents or chemicals to be ordered. Dr. Rachy Abraham answered many questions of mine and have given me valuable advice about my experiements. I also want to thank all other fellow labmates, Ashley Nelson, Rebecca Glowinski and Dr. Sreekumar Eswaran Potty for the stimulating discussions during the lab meetings. Outside of our lab, I would like to thank Dr. Anthony Leung and Dr. Yoshinari Ando, as they kindly provided their microRNA microarry data which inspired part of this project. Besides my advisor, I would also like to thank my other thesis reader Dr. Jay Bream, for agreeing to spend their valuable time reading this work and give me feedback on the thesis. Finally, I must express my very profound gratitude to my parents for providing me encouragement throughout my study at Hopkins.

Table of Contents

List of Tables and Figures

Introduction

Sindbis virus induced encephalomyelitis

Alphaviruses are a group of mosquito-borne, enveloped single-stranded, positive-sense RNA viruses that belong to the Togaviridae family. Encephalitic alphaviruses including Western, Eastern and Venezuelan equine encephalitis viruses (WEEV, EEEV and VEEV respectively) are New World alphaviruses endemic in the Americas [1]. Typical symptoms of New World alphavirus infections start with febrile illness, followed by evidence of acute neuroinvasive disease such as convulsion, coma, sensory deficits, muscle weakness, and even death [1, 2]. EEEV encephalitis, although transmitted to humans at a low rate in the United States, is the most lethal arboviral disease and has a case-fatality rate of 33% [3]. Patients that survive alphaviral encephalitis may also suffer from long-term neurological sequelae including cognitive, emotional, sensory and motor impairment [1, 2]. In contrast, Sindbis virus (SINV) and other Old World alphaviruses including Chikungunya virus (CHIKV), Ross River virus (RRV) and Semliki Forest virus (SFV) cause fever, malaise, rash and polyarthritis in humans and were mainly prevalent in Africa, East Asia and Europe [4], but one emerging and spreading worldwide Old World alphavirus has also been reported to affect the nervous system. Sporadic cases of CHIKV-induced neurologic diseases have been reported. For instance, in a CHIKV outbreak in western India, 16% of the patients showed encephalitis, myelopathy, or peripheral neuropathy [5, 6]. Currently, there are no specific antiviral therapeutics for alphaviruses; treatment is limited to supportive care. Several CHIKV human vaccine candidates are under development, but vaccines for the encephalitic alphaviruses have been licensed in horses but not for human use [2]. Therefore, understanding the pathogenesis of alphavirus-induced encephalomyelitis is critical for developing effective treatments and controls for neuroinvasive alphaviral diseases.

Although the prototype alphavirus SINV causes arthritis in humans, it shows neurotropism in mice and provides a useful model for studying the acute and chronic neuropathology of closely related encephalitic alphaviruses. SINV genome RNAs form nucleocapsid complexes

with capsid proteins (CPs), and are enveloped by host-derived lipid bilayers that contain 80 glycoprotein E1/ E2 trimers (Figure 1A) [7, 8]. Envelope proteins E1/ E2 mediate virus binding and entry into host cells [9, 10]. Low pH triggers fusion of the virus envelope with the endosome membrane and release of the viral genome. Non-structural proteins nsP1- nsP4 are translated from the 5' end of the positive-strand RNA genome in the cytoplasm (Figure 1B). In the late phase of infection, subgenomic mRNAs are transcribed from the 3' terminal structural region [8]. The polyprotein CP-pE2-6K-E1 or CP-pE2-TF is translated from the subgenomic RNAs is further processed into structural proteins CP, E1, E2 and two small membrane proteins 6K and TF [7].

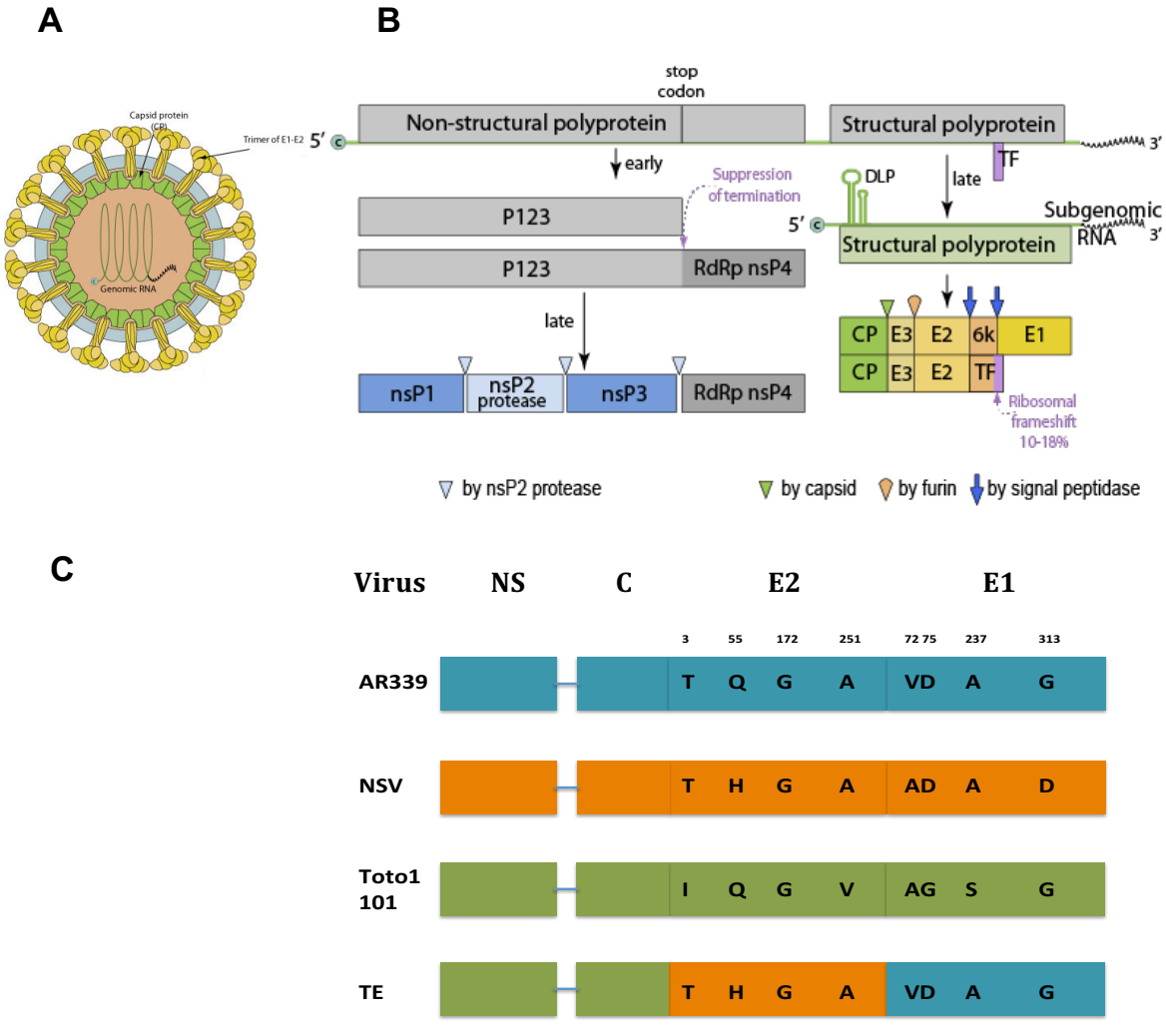

Figure 1. Alphavirus virion (A) and genome structure (B) and construction of the TE and NSV strains of Sindbis virus (C) [8, 11].

In mice, after intranasal or intracerebral inoculation SINV primarily infects and replicates in neurons of the central nervous system (CNS). SINV infections vary in disease severity, depending on the virus strain, the maturity of neurons and the genetic background of hosts [7]. The two strains of SINV used in this study, neuroadapted Sindbis virus (NSV) and TE, are both derived from the original low passage AR339 strain isolated from mosquitos in 1952. NSV was produced by serial passage in mice brains. The TE strain was constructed by recombination of Toto1101 cDNA clone of SINV with the NSV E2 glycoprotein fragment and the original AR339 E1 sequence (Figure 1C) [11]. Mutations of critical amino acids in SINV envelope proteins E1/E2, TF, nsP3 or the 5' nontranslated region are able to alter the neurovirulence of SINV [7]. AR339 and TE strains cause only mild disease in adult C57BL/6 mice, while the fatal NSV strain causes more than 90% mortality. Mice infected with NSV show signs of flaccid hindlimb paralysis 4 days post infection (dpi) and succumb within 7 to 10 dpi [12]. Newborn mice infected with TE also have shorter average survival time than those inoculated with AR339 [13]. The enhanced virulence of NSV and TE is partly due to the Histidine-55 substitution for Glutamine in glycoprotein E2 [14]. Additional mutations that appear in the NSV strain during neuroadaptation are associated with increased replication efficiency, more intense inflammatory response and neuronal damage in the brain and spinal cord. [7]

AR339 and TE strains cause nonfatal encephalitis in adult mice, while infection of younger weanling or newborn mice leads to fatal encephalomyelitis. The age- dependent decrease in SINV susceptibility is primarily due to the intrinsic resistance of mature neurons rather than the development of the immune system [7]. Previous work in our lab has shown that neuronal maturity is associated with increased baseline mRNA levels of interferon regulatory factor (IRF)-3, IRF7, interferon (IFN)-β and several IFN-stimulated genes (ISGs) [15]. Undifferentiated neurons also express a dominant negative γ isoform of IRF7, which switches to the full-length active isoform in mature neurons. More rapid activation of IFN and ISGs in mature neurons thus restricts virus replication and SINV-induced neuronal apoptosis [15].

These findings also emphasized the importance of innate immune signaling in controlling SINV infection.

Toll-like receptor signaling during neurotropic virus infection

Several families of viruses, including alphaviruses, flaviviruses (eg. West Nile (WNV), Japanese encephalitis (JEV), St Louis encephalitis (SLEV) and tick-borne encephalitis), enteroviruses (eg. Enterovirus 71, poliovirus), rhabdoviruses (eg. rabies, vesicular stomatitis virus (VSV)), bunyavirus (eg. La Crosse (LACV)) and herpesviruses (eg. herpes simplex (HSV)) may invade and cause irreversible damage in the terminally differentiated neurons of the CNS [16]. As neurons are nonrenewable, the CNS must be protected from viral infections by tightly regulated immune responses [16, 17]. The innate immune response to neurotropic virus infection is important for the initial pathogen recognition, effective restriction of virus propagation and induction of proinflammatory genes. Detection of conserved pathogen associated molecular patterns (PAMPs) is mediated by four groups of pathogen recognition receptors (PRRs): Toll-like receptors (TLRs), RIG-I like receptors (RLRs), NOD-like receptors (NLRs), and cytosolic DNA sensors. PRR activation pathways converge on the activation of transcription factors including IRF3, IRF7 and NF□B, and induction of proinflammatory genes (Figure 2) [17, 18].

Surface or endosomal membrane bound TLRs are capable of recognizing a wide range of PAMPs via their N-terminal leucine-rich repeats. Viral nucleic acids are the dominant PAMPs of viruses and can be detected by the endosomal TLRs: TLR3 detects double-stranded RNA, TLR7/ TLR8 recognizes single-stranded RNA, unmethylated DNA activates TLR9 and mouse TLR13 is reported to bind bacterial ribosomal RNAs [19]. Upon TLR engagement, the cytoplasmic Toll/ IL-1R homology (TIR) domain mediates recruitment of TIR-containing adaptor proteins. All TLRs require the prototype TIR family adaptor MyD88 (myeloid differentiation primary response 88) for signal transduction, except for TLR3 that utilizes the adaptor TRIF (TIR domain containing adaptor inducing IFN-β). TIR family

adaptors activate I□B kinase-□ (I□□-□) and TANK binding kinase 1, which then induce activation of mitogen-activated protein kinases (MAPKs), NF□B and IRFs. These lead to the production of type I IFNs, proinflammatory cytokines, chemokines and other antiviral genes [17-19]. TLR signaling provides protection against multiple neurotropic viruses including WNV, JEV, poliovirus, VSV and HSV in mice, mainly by stimulation of IFN expression and control of virus replication [17, 18].

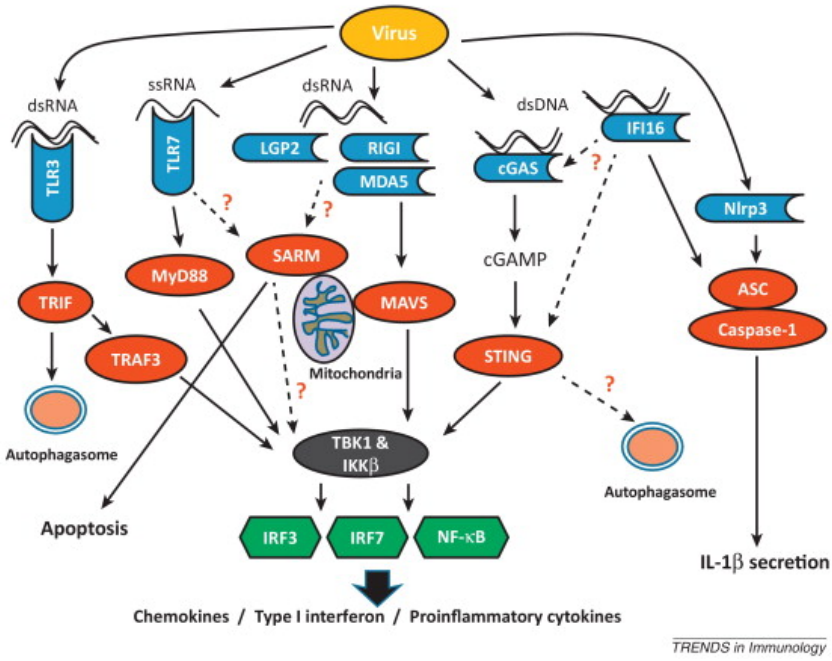

Figure 2. Innate immune responses to virus infection in the central nervous system [18]. Detection of viruses in the CNS can be mediated by one of four types of PRRs: TLRs, RLRs, cytosolic DNA sensors or NLRs. TLR engagement activates MyD88 or TRIF-dependent signaling pathways that drive nuclear translocation of IRF3, IRF7 and nuclear factor (NF)-□B and induce expression of type I IFNs and proinflammatory cytokines (such as pro-IL-1□ and pro-IL-18). RLRs include retinoic acid-inducible gene I product (RIG-I), melanoma differentiation-associated antigen 5 (MDA5), and laboratory of genetics and physiology 2 (LGP2) that recognize double-strand RNA with blunt ends. Activated RIG-I and MDA5 interact with mitochondrial antiviral signaling protein (MAVS), which also activate the transcription factors IRF3, IRF7 and NF□B. LGP2, however, serves as a negative regulator of RLR pathways. DNA from viruses such as HSV may binds and activates the cytosolic DNA sensor cGAS (cyclic GMP-AMP synthase), which catalyzes the synthesis of cyclic guanosine monophosphate-adenosine monophosphate (cGAMP). This second messenger and another DNA sensor Interferon gamma-inducible protein 16 (IFI16) can activate stimulator of interferon genes (STING) and mediate downstream proinflammatory responses. Finally, viral nucleic acids or infection-induced cellular stress can activate the cytosolic NLR inflammasomes. For instance, NOD-like receptor family pyrin domain-containing 3 (NLRP3) activation and oligomerization lead to the activation of caspase-1, which subsequently convert pro-IL-1□ and pro-IL-18 to their mature forms. SARM1, a newly discovered TIR domain containing protein, can either mediate cytokines and chemokines secretion via currently unknown pathways or trigger cell death in response to certain viruses.

Recent studies show that TLR activation may also contribute to viral disease pathogenesis. For instance, the rhabdovirus rabies virus infection causes fatal encephalitis in wild-type mice, while TLR3 deficient mice have lower viral load and higher survival rate [18]. TLR-associated neuropathology can also be mediated by SARM1 (Sterile alpha and TIR motif-containing protein1), the fifth member of TIR family adaptors, which also include the well-studied MyD88, MYD88-adaptor-like protein (MAL), TRIF and TRIF-related adaptor molecule (TRAM) [18-20]. SARM1 is evolutionarily conserved and mammalian SARM1 is predominantly expressed in the CNS, and mainly in neurons rather than glial cells. Unlike other TIR family members, SARM1 was first identified as a negative regulator of TRIF-dependent TLR signaling [20]. Though the functions of SARM1 remain to be elucidated, it has been shown lately that SARM1 also regulates axon degeneration in mouse, *Caenorhabditis elegans* and *Drosophila*. Furthermore, SARM1 correlates with neuronal death under the stress of oxygen and glucose deprivation, mitochondria destruction, or viral infections [18-22]. In the *C. elegans* model of amyotrophic lateral sclerosis, activation of *tir-1*, the SARM1 ortholog, and its downstream signaling pathway are implicated in non-apoptotic motor neuron degeneration, suggesting SARM1 may play a conserved role in neurodegeneration [23]. How these processes occur has yet to be understood. One study shows that TLR7/ TLR9 stimulation with agonists induces SARM1 upregulation and aggregation in the mitochondria and triggers apoptosis of primary cortical neurons, suggesting that SARM1 signaling may contribute to viral pathogenesis in the CNS [24]. In addition, Mukherjee *et al*. reported that MAVS activation upon LACV infection stimulates SARM1-dependent mitochondrial damage and neuronal apoptosis *in vivo* [25]. Apart from mediating neuronal death directly, SARM1 signaling also contributes to cytokine production and immune-mediated neurodegeneration in the brain during VSV infection [26].

Identification of microRNAs (miRNAs) as unconventional TLR ligands also elucidated a novel TLR-dependent neuropathogenic pathway. MiRNAs are small non-encoding RNAs of about 22 nucleotides and are capable of regulating gene transcription and translation. Recent

studies suggest that some miRNAs structurally mimic viral RNA, directly bind and activate TLR signaling cascades in neighboring cells [27, 28]. It has been hypothesized that expression disturbance of specific miRNAs are associated with neurotoxicity during the course of virus infections and neurodegenerative diseases [29]. For instance, miR-21 is upregulated in macrophage-secreted vesicles (EVs) in HIV/ SIV (human or simian immunodeficiency virus) infected brains [30, 31]. Although the trafficking mechanism is not well understood, miR-21 contained in EVs activates the endosomal TLR7 pathway and induces neuron cell death, which can be inhibited by a necroptosis inhibitor, necrostatin-1 [30]. Additionally, TLR7 activation by let-7b, a miRNA upregulated in the cerebrospinal fluid of patients with Alzheimer's disease, also induces neurodegeneration in mouse models [32]. Therefore, we are interested in the involvement of endosomal TLR signaling pathways during SINV infections, which can be either protective or pathogenic in the CNS.

Differential upregulation of endosomal TLRs in the brain by several alphaviruses, including VEEV, neurovirulent CHIKV E1: A226V and SFV, has been reported [33-35]. Regulation of these TLRs and associated TIR adaptors during SINV infections has not been studied. Especially, we would like to know whether SINV induces SARM1 and/ or miRNA dysregulation, which may contribute to immune-mediated pathogenesis. Keeping these in view, the present study has compared the expression of endosomal TLRs and SARM1 during infections with fatal and nonfatal strains of SINV. Based on microarray analysis performed by Dr. Yoshinari Ando, miR-21a and miR-146a are induced more than 2 fold by TE infection at 5 dpi. We want to confirm the results and examine the expression patterns of these two miRNAs, using semi-quantitative real-time polymerase chain reactions.

Sindbis virus induced neuronal cell death

Apoptosis is the first recognized programmed cell death (PCD) pathway and is a crucial mechanism for homeostasis and development in multicellular organisms. Characteristic morphology changes in apoptotic cells include cytoplasmic shrinkage, nuclear condensation, DNA fragmentation, plasma membrane blebbing and formation of apoptotic bodies. These hallmarks can be distinguished from necrosis, which occurs with increased cell volume, organelle swelling, cell rupture and release of cellular content [36].

Apoptosis is a tightly controlled process and can be triggered by either extrinsic stimuli of death receptors or intrinsic cellular stress. Death receptors, for instance, TNFR and FAS receptor ligation induces assembly of intracellular DISC (death inducing signaling complex), which then recruits adaptor proteins such as FAS-associated death domain (FADD) via death domains and directly cleaves pro-caspase-8 into active caspase-8 [37]. Intrinsic stresses such as DNA damage, oxidative stress and excessive Ca^{2+} influx induce sequestration of anti-apoptotic B-cell lymphoma 2 (BCL-2) by BH3-only proteins, which allows pro-apoptotic BAX or BAK translocation to mitochondria and formation of mitochondrial membrane permeability pores. Multiple pro-apoptotic proteins including cytochrome c, apoptosis inducing factor (AIF) and endonuclease G then release into cytoplasm from mitochondria. Cytochrome c induces "apoptosome" formation by recruiting apoptosis protease activating factor-1 (APAF-1) and activates caspase-9 [37]. Executioner caspase-3 and caspase-7 are subsequently activated by caspase-8 or -9 and induce apoptotic cell death by proteolysis of specific cellular targets such as transcription factors, kinases and Poly (ADP-ribose) polymerase 1 (PARP1). Chromosomal DNA fragmentation, one of the apoptotic hallmarks, is mediated by endonucleases [37].

SINV infection induced apoptosis *in vitro* occurs in multiple immortalized cell lines (such as BHK-21 cells, NSC-34 cells and N18 neuroblastoma) and cultured primary cortical neurons [38-40]. SINV- induced apoptosis is initiated during virus entry and acid-driven fusion with the cell membrane [38]. This apoptotic cell death is associated with caspase-3 activation and

PARP-1 cleavage and can be inhibited by the pancaspase inhibitor zVAD-FMK (N-benzyloxycarbonyl-Val-Ala-Asp-fluoromethyl ketone) and anti-apoptotic proteins (such as Bcl-2, Beclin-1) overexpression [38, 41].

The ability to induce apoptotic neuron death in the brain and spinal cord of newborn mice correlates with the neurovirulence of SINV. In adult mice, however, spinal cord motor neuron death appears to employ a non-apoptotic mechanism [12, 40, 42]. Intracerebral inoculation with NSV strain leads to neuronal cell death mainly in the hippocampal and lumbar spinal cord regions and results in acute flaccid paralysis as well as lethality. Both apoptotic cells that are positive for activated caspase-3 and TUNEL (Terminal deoxynucleotidyl transferase dUTP nick end labeling) and necrotic cells that are sometimes adjacent to the apoptotic neurons can be observed in the brains of infected mice. In contrast, motor neuron degeneration in the anterior horns of spinal cord is mainly necrotic, with an absence of caspase-3 activation, enlarged nuclei, swollen organelles and loss of membrane integrity [12]. Additionally, overexpression of BCL-2 family proteins, BCL-2 and BAX, inhibits hippocampal neuronal death and fatal disease in NSV-infected adult mice, but cannot prevent lumbar motor neuron destruction or the onset of hindlimb paralysis [43]. Recent studies in our lab also demonstrated that TE infection could also induce necrosis of spinal cord motor neurons in IRF7$^{-/-}$ mice, which parallels the onset of hindlimb paralysis by 5 dpi. The ratio of cleaved caspase-3 to TUNEL positive cells in the spinal cord was lower than that observed in the brain, suggesting that caspase-3-independent cell death occurred in the spinal cord of IRF7$^{-/-}$ mice. Therefore, it is believed that SINV infection can activate divergent cell death pathways in different types of neurons. Necrotic motor neuron death occurs not only in alphaviral encephalomyelitis, but also in other motor neuron diseases that may include other infectious acute flaccid myelitis and motor neurodegenerative diseases such as ALS. Therefore, understanding its mechanism is of interest to us.

Regulated necrosis: necroptosis

PCD used to be a synonym of apoptosis, whereas necrosis was considered to be a form of accidental cell death in response to irreversible physicochemical injury. However, accumulating genetic, biochemical and physiological evidence unmasked multiple neglected non-apoptotic PCD mechanisms and redefined the dichotomy of cell death into three categories: apoptosis, autophagic cell death and necrosis [36, 44-46]. The discovery of specific genetic programs and chemical inhibitors also revealed the existence of regulated necrosis, which is tightly regulated like other PCDs. Several modes of regulated necrosis, including necroptosis, pyroptosis, parthanatos, MPT-RN (mitochondrial permeability transition- mediated regulated necrosis), ferroptosis/ oxytosis and NETosis (neutrophil extracellular trap release-associated cell death), have been proposed based on their unique underlying signaling pathways (Figure 3), though they share similar morphological features of necrotic cells [36, 44-46].

Necroptosis is the prototype and best characterized regulated necrosis pathway, and the earliest evidence for this pathway was observed in tumor cells that undergo tumor necrosis factor-α (TNFα)-induced, caspase-antagonized cell death. The identification of RIP1 and RIP3 (receptor-interacting serine/threonine-protein kinase 1 and 3) as crucial regulators of TNFα induced necrosis, and the specific inhibitory effect of a RIP1 inhibitor necrostatin-1 further provided evidence that necroptosis was a programmed necrosis pathway. A variety of intracellular and extracellular triggers, for instance, TNFα family receptor ligands, PAMPs, DNA damage, T-cell receptor ligation and IFNs, have been reported. Under apoptosis deficient conditions, such as FADD knockout or caspase-8 inhibition, these signals initiate the formation of a 'necrosome' containing RIP1, RIP3 and the downstream substrate MLKL (mixed lineage kinase domain like) that executes necroptosis [36, 44-46].

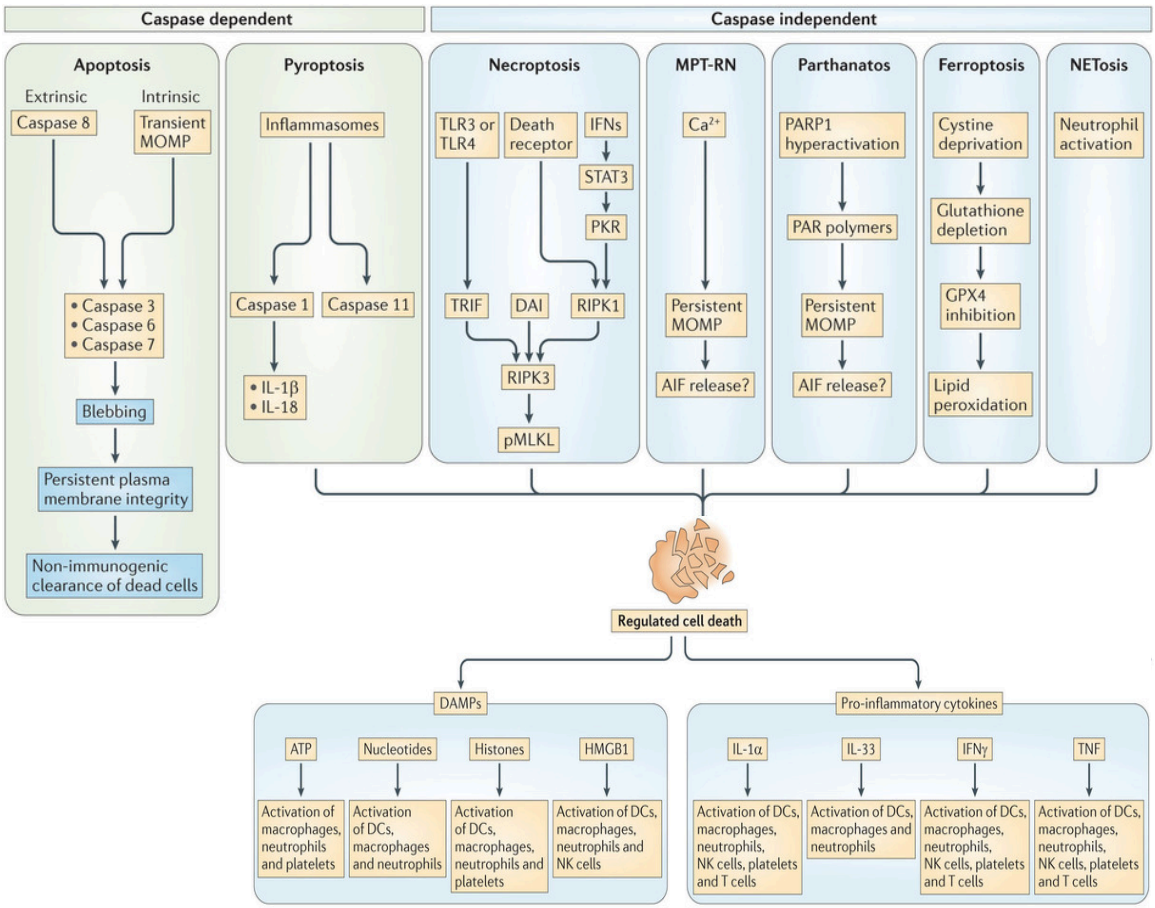

Figure 3. Regulated cell death pathways [45]. Apoptosis is the classical caspase-3 mediated PCD, induced by either extrinsic death receptor stimuli or intrinsic mitochondrial stress. Apoptotic cells progressively dissemble with relatively persistent membrane integrity and limited PAMPs release, and are generally considered non-immunogenic. Regulated necrosis (RN) pathways include caspase-dependent pyroptosis and caspase-independent necroptosis, MPT-RN, parthanatos, ferroptosis/ oxytosis and NETosis. Pyroptosis depends on inflammasome formation that activates pro-caspase-1 and -11. Cleaved caspases then induce osmotic swelling of the cells and release of proinflammatory IL-1 and IL-18. Necroptosis is the prototype form of caspase-independent regulated necrotic cell death. This pathway can be induced by signaling from death receptors, PRRs and IFNs and is mediated by sequential activation of RIP3 and MLKL. The term MPT-RN describes the form of regulated necrosis associated with cyclophilin D (CYPD) mediated mitochondrial outer membrane permeabilization (MOMP). Parthanatos involves hyperactivation of PARP1 and accumulation of PARylated target proteins. NAD^+ consumed by massive PARylation reactions and AIF (induces apoptosis-inducing factor) release triggered by PAR polymers lead to energy crises and necrotic cell death. Ferroptosis and oxytosis are two overlapping cell death-modalities that occur when the system X_C^- Cys/Glu antiporters are inhibited. Reduced levels of intracellular L-Cys results in glutathione (GSH) depletion and consequently GSH peroxidase 4 (GPX4) inhibition and lipid peroxidation. Ferroptosis is associated with iron-dependent reactive oxygen species (ROS) generation, lipid peroxidation and lysosomal membrane permeabilization (LMP). Glutamate excitotoxicity induced neuronal necrosis is typically classified as oxytosis, and it depends on calcium-dependent calpain activation rather than iron metabolism. NETosis, as its name suggests, requires the release of NET (neutrophil extracellular trap) that contains neutrophil chromatin, histone and other intracellular proteins. Unlike apoptosis, regulated necrosis pathways are characterized by cell rupture, the release of PAMPs and proinflammatory cytokines. Therefore, necrotic cells are generally considered as stronger inflammation inducers than apoptotic cells.

Extensively studied TNFα induced cell death exemplifies the crosstalk between apoptosis and necroptosis (Figure 4) [46]. TNFR1 trimerization induces pro-inflammatory responses by forming complex I comprising TNFR1-associated death domain protein (TRADD), ubiquitinated RIP1 and other components and activating NF□B/ MAPK pathway. In sensitized cells, deubiquitination of RIP1 by deubiquitinating enzyme cylindromatosis (CYLD) destabilizes complex I, and initiates the association of FADD, pro-caspase 8 and FLICE- like inhibitory protein long isoform ($FLIP_L$). Formation of TRADD- dependent complex IIa or RIP1- dependent complex IIb allows caspase-8 dependent apoptosis. $FLIP_L$ and pro-caspase-8 heterodimer also serves as a brake of necrosome or complex IIc assembly by proteolysis of CYLD, RIP1 and RIP3. When caspase-8 is inhibited by viral encoded inhibitors (such as CrmA and vIRA) or synthetic inhibitors (such as zVAD-FMK) and RIP3 and MLKL are expressed at sufficiently high levels, TNFα tends to induce necroptosis. RIPK1 and RIPK3 associate via their RHIM (RIP homotypic interaction motif) domains; trans- and auto-phosphorylated RIP1 and RIP3 then associate in an amyloid- like necrosome, recruit and phosphorylate the downstream executor MLKL. Activated MLKLs trimerize through exposed amino-terminal coiled-coil domain and translocate to the plasma membrane, possibly leading to ion influx-dependent necroptotic death [36, 44-46].

Apart from death receptors, PAMPs can also induce necroptosis through PRRs. With the presence of caspase inhibitor zVAD-FMK, stimulation of TLR3 by poly(I:C) or TLR4 by lipopolysaccharide (LPS) will recruit RIP3 through the RHIM-containing adaptor protein TRIF and induce either RIP1-dependent or independent necroptosis [36]. Another RHIM domain-containing protein, DAI (DNA-dependent activator of IFN regulatory factors), also recognizes viral double strand DNA and leads to RIP3- dependent necrosome formation during MCMV infection [47]. Recent studies also found that cytosolic RIG-I and STING pathway activation (by Sendai virus and MHV68, respectively) can mediate necroptosis in L929 cells [48].

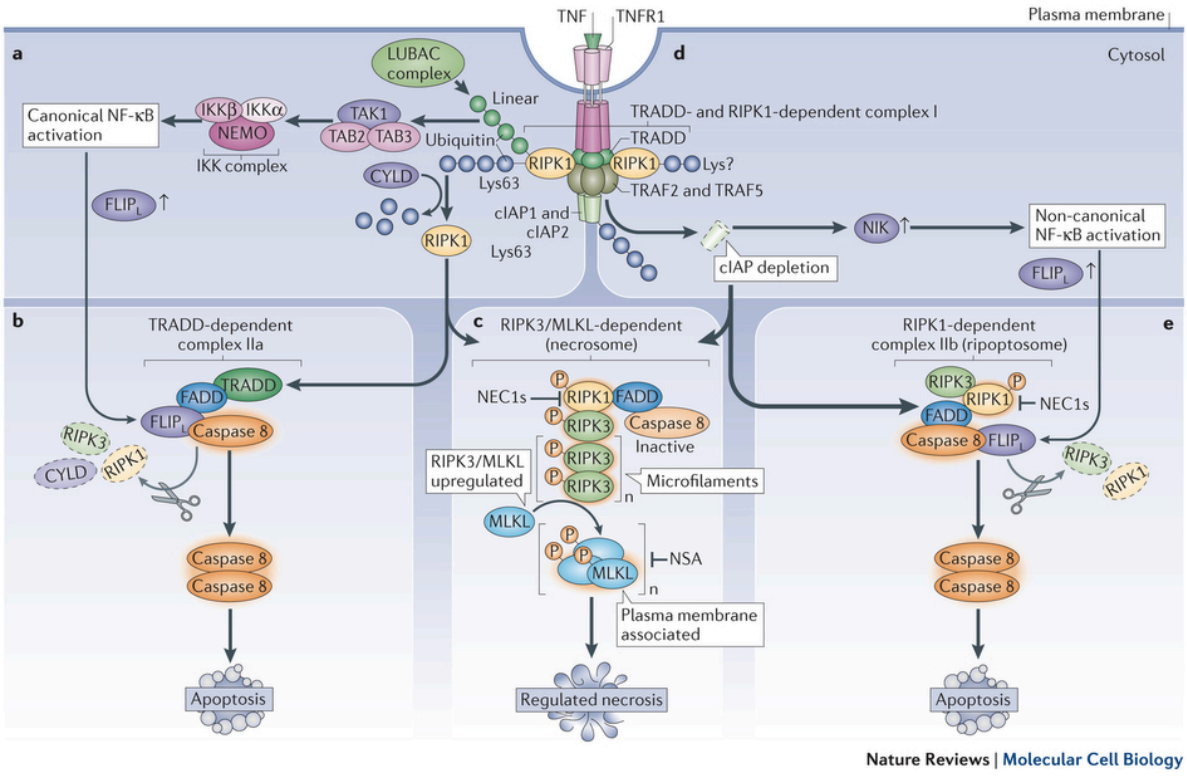

Figure 4. TNF induced apoptosis and necroptosis pathway [47].

Necroptosis is generally considered a more potent inflammation inducer than apoptosis, owing to the more acute and massive release of damage associated molecular patterns (DAMPs) from necrotic cells (Figure 3) [36, 45]. Although no necroptosis- specific DAMPs have been discovered so far, DAMPs such as HMGB1 (high-mobility group box 1), IL-1 family cytokines, S100 proteins a9 and mitochondrial DNA (mtDNA) were found to be upregulated in necroptotic tissues. These DAMPs may then provoke and amplify inflammatory responses, and possibly lead to immunopathology. For instance, RIP3 and MLKL are overexpressed in inflamed ileum and colon tissues of patients with inflammatory bowel disease; necroptosis induces IL-1, IL-8 and HMGB1 secretion in colonic HT-22 cells and contributes to inflammation [49, 50].

Accumulating evidence has implicated necroptosis in the pathogenesis of various diseases, including neurological disorders such as ischemic or hemorrhagic stroke, traumatic brain injury (TBI), spinal cord injury (SCI), Alzheimer's, multiple sclerosis, amyotrophic lateral sclerosis (ALS) and other neurodegenerative diseases [51]. On one hand, necroptosis can be

the regulated necrosis mechanism of neurons; on the other hand, necroptotic microglia and oligodendrocytes may exacerbate pathogenic immune responses. Incubation with 1 ng/ml TNFα and 50 μM zVAD-FMK for 4 h *in vitro* can efficiently induce necroptotic cell death in the hippocampal neuron cell line HT-22, suggesting that molecular machinery of necroptosis exists in neurons [52]. Necroptosis also contributes to motor neuron death in experimental models of ALS. In lower spinal cord from human ALS pathological samples, Ito *et al*. observed upregulation and phosphorylation of necroptosis regulators RIPK1, RIPK3 and MLKL, especially in the region that displays axonal pathology [53]. Additionally, upregulation of these necroptotic markers RIP1, RIP3 and MLKL were observed in the spinal cords in both mSOD1 (misfolded superoxide dismutase 1) and Optineurin knockout mouse models of ALS [53]. Furthermore, the protective effects of RIP1 inhibitor necrostatin-1 and MLKL antagonist necrosulfonamide (NSA) for motor neurons *in vitro* and *in vivo* confirm the involvement of necroptosis in ALS pathogenesis [54]. Increased expression levels of RIP3, MLKL and HMGB1 were also present in spinal cords following traumatic injury; necrostatin-1 inhibits motor neuron death in SCI without affecting apoptosis [55, 56]. Taken together, necroptotic cell death can be involved in motor neuron degeneration, which is exemplified in the case of ALS and SCI.

Virus-induced necroptosis has also been described following infections with both DNA viruses (including MHV68, HSV and vaccinia virus) and RNA viruses (including HIV, IAV, JEV, Sendai virus and reovirus) [57-62]. DNA viruses, for example, vaccinia virus may sensitize host cells to TNF-dependent necroptotic death by encoding a caspase-8 inhibitor B13R [60]. Otherwise, MCMV and MHV68 infection can induce necroptosis by activating the DNA sensors DAI and STING pathways respectively; HSV-1 and HSV-2, on the other hand, encode viral RHIM-containing proteins ICP6 and ICP-10, which directly engage the RIP1/ RIP3 necrosome [61]. The mechanisms of RNA virus activated necroptosis are less studied: IAV activates necroptosis via DAI and Sendai virus triggers necroptosis via RIG-I [57, 62]. Besides, the production of IFN- and *de novo* synthesis of viral RNA are both

required for activation of necroptosis signaling cascade during reovirus replication in L929 cells [59].

It has been shown that necroptosis can be protective *in vivo* by restricting virus propagation and coordinating immune responses, and viruses such as HSV1 and MCMV encode viral inhibitors of necroptosis to block this antiviral cell death [47, 61]. Interestingly, mutant human coronavirus strain OC43 (HCoV-OC43), which has enhanced neurovirulence, astrogliosis and mortality in mice, induces increased mRNA transcription of RIP1 and RIP3 compared to the wild-type virus, without affecting their protein levels. Besides, RIP1 knockdown and the MLKL antagonist NSA prevents HCoV-OC43- induced cell death of human neuroblastoma cells and primary mouse CNS cultures [63]. Another encephalitic virus, JEV, is also shown to induce MLKL upregulation in neurons both *in vitro* and *in vivo*. Deletion of MLKL delays the onset of JE and alleviates the symptoms, at least partly due to reduced levels of inflammatory cytokines [58]. These lead to the hypothesis that HCoV-OC43- or JEV- induced necroptosis contributes to neuroinflammation and CNS damage.

Here we sought to understand whether regulated necrosis contributes to the pathogenic inflammation and motor neuron degeneration during SINV infection. Considering the involvement in neurologic disorders and the best-characterized molecular mechanism, we would start by looking into evidence for the necroptosis pathway. Earlier studies demonstrated that TNF, the prototype necroptosis inducer, is upregulated in the brain and spinal cords of SINV-infected mice [64]. Besides, TNFα and TNFR deficient mice exhibit more resistance to NSV-induced brainstem and cervical motor neuron cell death as well as decreased mortality [65, 66]. Therefore, I will evaluate the presence of necroptotic cell death in SINV- infected NSC-34 cell line and in mouse spinal cord, using RIP3 upregulation as an indicator.

Materials and Methods

NSC34 cells culture and differentiation

The murine NSC34 cell line was a hybrid of N18TB2 neuroblastoma cells and embryonic mouse spinal cord motor neurons and was kindly provided by Dr. Neil Cashman (University of Toronto, Canada). Cells were maintained at 37°C in 5% CO_2 in growth medium that contains Dulbecco's modified Eagle's medium (DMEM) supplemented with 10% heat inactivated fetal bovine serum (FBS), 1% penicillin/ streptomycin (Gibco), 1% L-Glutamine (Gibco) and were subcultured every 3 days.

For differentiation, NSC34 cells were plated at a density of 5 x 10^4 cells/ cm^2 in 6 well plates with or without matrigel (Becton-Dickinson Biosciences) coating. One day after plating, growth medium was exchanged for 1:1 DMEM/ Ham's F12 (Gibco) with 1% FBS, 1% penicillin/ streptomycin, 1% L-Glutamine, 1% modified Eagle's medium nonessential amino acids (MEM-NEAA) and 10 mM all-trans retinoic acid (Sigma-Aldrich). Cells were differentiated for up to four days and differentiation medium was changed every 2 days.

In vitro viral infection

Cell viability was determined using trypan blue exclusion. TE virus stocks of 2.5 x 10^9 plaque forming unit (pfu)/ ml were titered on BHK cells and were diluted in DMEM with 1% FBS to the designated multiplicity of infection (MOI). Undifferentiated cells seeded for 24 hours or differentiated cells were incubated with the virus for 1 h in appropriate conditions and the plates were rocked every 15 min. After washing with PBS, the virus containing media was then replaced with fresh DMEM with 1% FBS.

Plaque assay

Supernatant fluids were collected from culture media 0, 8, 12, 24, 48 and 72 hours post infection (hpi) and frozen at -80°C. BHK cells were plated one day before the experiment. Cell monolayers were washed with PBS and were then infected with 200 µl of serially diluted

supernatant fluids. After 1 h incubation and regular rocking, cells were overlaid with bacterose agar with 50% MEM and 8% FBS. After agar solidified at room temperature, BHK cells were incubated at 37°C for approximately 2 days, and were stained with neutral red for counting the number of plaques.

In vivo viral infection and tissue collection

Four to six week old wild-type C57BL/6 mice were anaesthetized with isoflurane and intracranially (i.c.) inoculated with 1000 pfu of either TE or NSV virus suspended in 20 µl of PBS by Dr. Victoria Baxter. Similarly, $IRF3^{-/-}$ and $IRF7^{-/-}$ mice were i.c. infected with 1000 pfu of TE virus by Elizabeth Troisi.

For brain and spinal cord collection, mice were deeply anaesthetized and perfused with 15 ml ice-cold PBS. Small intestine was also harvested from uninfected C57BL/6 mice, used as positive control for western blot analysis of RIP3. All tissue samples were snap-frozen in liquid nitrogen, stored at - 80°C and supplied to me by either Dr. Baxter or Elizabeth Troisi.

All mouse experiments were performed in accordance with protocols approved by the Johns Hopkins University Animal Care and Use Committee.

Total RNA extraction

For RNA extraction from brain and spinal cord, tissue samples were homogenized in TRIzol reagent (Invitrogen) and were centrifuged at 12,000 ×g for 10 min at 4°C. The supernatant fluid was mixed with chloroform thoroughly and incubated at room temperature for 3 min. The upper aqueous layer was then separated by centrifugation at 12,000 ×g for 15 min and collected in new tubes. Following isopropanol precipitation, RNA pellets were washed twice with 75% ethanol and air dried for 10 min. After resuspension in DNase/ RNase-free DEPC water, RNA concentrations were determined using NanoDrop Spectrophotometer ND-1000.

Semi-quantitative RT-PCR analysis of mRNA and microRNA

For mRNA expression analysis, 4 μg of RNA were reverse transcribed into cDNA utilizing the High Capacity cDNA Reverse Transcription Kit (Applied Biosystems) and an Applied Biosystems 2720 thermal cycler. Real-time PCR was then performed using EagleTaq Universal Master Mix w/ ROX (Roche, 07249926190) and specific PrimeTime predesigned primer and probe sets obtained from Integrated DNA Technologies (Table 1). The PCR conditions were 50°C for 2 min, 95°C for 10 min, and 50 cycles of 95°C for 15 s, and 60°C for 1 min. Transcript levels of target genes were normalized to the endogenous levels of GAPDH mRNA and fold changes relative to the uninfected controls were calculated using $2^{-\Delta\Delta Ct}$ method.

Gene	Assay ID	Reference Seq no.
Mouse Tlr3	Mm.PT.58.8085919	NM_126166(1)
Mouse Tlr7	Mm.PT.58.10526075	NM_133211(1)
Mouse Tlr8	Mm.PT.58.16021150	NM_133212(1)
Mouse Tlr9	Mm.PT.58.5114450	NM_031178(1)
Mouse Myd88	Mm.PT.58.33389595	NM_010851(1)
Mouse Sarm1	Mm.PT.58.41336232	NM_001168521(2)
Mouse Rip3	Mm.PT.58.33227794	NM_001164108(3)
Mouse Mlkl	Mm.PT.58.16870825	NM_029005(1)
Rodent Gapdh	Rodent GAPDH forward primer / Rodent GAPDH reverse primer / Rodent GAPDH Probe (VIC) (Applied Biosystems)	

Table 1: Primers used for RT-PCR analysis

For miR-21 and miR-146 expression analysis, 10 ng of total RNA were reverse transcribed into cDNA using TaqMan Advanced miRNA cDNA Synthesis Kit (Cat. no. A28007),

according to the manufacturer's protocol. Quantification of miRNAs was performed using TaqMan Advanced miRNA Assays (Applied biosystems, Cat. no. A25576) listed in Table 2 and TaqMan Fast Advanced Master Mix (Cat. no. 4444556). Each sample was analyzed in duplicate and normalized to the expression levels of let-7c.

Assay Name	Assay ID
hsa-miR-21-5p	478399_mir
hsa-miR-146a-5p	478577_mir
has-let-7c-5p	477975_mir

Table 2: Taqman MicroRNA assays used for miRNA RT-PCR analysis

Western blot analysis

NSC34 cells and mouse tissue were homogenized by sonication in RIPA buffer (50 mM Tris, 150 mM NaCl, 1% NP-40, 0.5% Sodiumdeoxycholate, 1 mM EDTA and 0.1% SDS) supplemented with protease inhibitor cocktail (Sigma) and phosphatase inhibitor (Sigma), and incubated on ice for 30 min. Supernatant fluid was harvested after centrifugation at 12,000 rpm for 15 min at 4°C and stored at - 80°C. The concentrations of total proteins were determined using DC Protein Assay (Bio-rad). Samples were boiled in 6x cracking buffer (0.5 M Tris, 10% sodium dodecyl sulfate, 30% glycerol, 6% β-mercaptoethanol and 0.12% bromophenol blue) for 5 min. For RIP3 expression level analysis, 150 µg protein from brain and spinal cord homogenates, 40 µg protein from small intestine samples or 20 µg of protein from NSC34 cell lysate per well was resolved using 4-20% Tris-Glycine Universal gels (NuSep Cat. No. NG11-420). Proteins were transferred to nitrocellulose membrane (Bio-rad) in 10% methanol transfer buffer, and blocked with 5% non-fat skim milk in Tris buffered saline with 0.1% Tween 20 (TBS-T) for 1 h at room temperature. Membranes were then incubated in anti-RIP3 antibody (1: 1000, Cell signaling D4G2A or Abcam ab56164) or anti-β-actin (1: 10000, Cell signaling) in TSB-T with 5% BSA at 4°C overnight. After washing 3

times in TBS-T for 5 min, membranes were then incubated with either goat anti-rabbit (1: 2,000) or anti-mouse (1: 10,000) horseradish peroxidase (HRP)-conjugated secondary antibody for 1 h at room temperature. Following 5 washes with TBS-T buffer, chemiluminascence signals were developed using the ECL Western blotting detection reagent (GE Healthcare Life Sciences).

Immunohistochemistry staining

Paraffin-embedded, paraformaldehyde-fixed sections were heated at 60°C for 10 min and then rehydrated by successive immersion in xylene, 100% ethanol, 95% ethanol, 70% ethanol, and running tap water, respectively. Sections were boiled in 10 mM Sodium citrate buffer (pH = 6) for 8 min for heat-induced antigen retrieval by a microwave, cooled for 20 min, and washed three times in TBS with 0.025% Triton-X. Endogenous peroxidase activity was quenched using freshly prepared 3% hydrogen peroxide in methanol for 10 min. Tissues were then blocked in 1x PBS with 0.04% Triton-x and 10% Normal Goat Serum (NGS) for 30 min. After overnight incubation with anti-RIP3 antibodies (1: 200 in 1x PBS with 0.04% Triton-x and 5% NGS, Abcam ab56164) at 4°C in a humidified chamber, slides were washed with TBS/ Triton-x wash buffer for 3 times and stained with biotinylated anti-rabbit IgG antibody (1: 300 dilution, Vector Laboratories, Cat. no. BA-1000) for 40 min at room temperature. Sections were then incubated in VECTASTAIN Elite ABC reagents (Vector Laboratories, Cat. no. PK-6100) for 40 min and developed in DAB solution (Vector Laboratories, Cat. no. SK-4100) for 8 min. Finally, slides were counterstained with 1: 10 hematoxylin for 1 min, dehydrated, and mounted with Permount.

Statistical analysis

Two-way ANOVA with Bonferroni post-tests was used to compare the difference among different groups during the course of infection. Data were presented as mean ± standard error. The differences were considered statistically significant when p-value < 0.05. All statistical analysis was performed using GraphPad Prism 5.

Results

Endosomal TLRs and downstream adaptors are upregulated by SINV in wild-type B6 mice

The NSV strain is known to cause lethal immune-mediated encephalomyelitis in wild-type adult C57BL/6 (B6) mice, while TE infection causes only mild disease. As endosomal TLRs are capable of recognizing viral nucleic acids, and are implicated in immune responses of several neurotropic viruses, we would like to know whether these TLRs are associated with the severity of SINV-induced disease. Considering the divergent cell death pathways activated by SINV in the brain and spinal cords, we would also examine TLR expression at both regions. Therefore, mRNA expression of endosomal TLRs in the brain and spinal cords following TE or NSV infection were compared by semi-quantitative RT-PCR. The mRNA levels of TLR3, TLR7, TLR8 and TLR9 were all significantly increased during the seven-day course of infection, by both TE and NSV strains of SINV (Figure 5A). Similar transcription profiles were observed in the brain and spinal cord. TLR3 expression peaked during 3 to 5 dpi and was increased by about 10-fold and 5-fold by the NSV and TE strains respectively ($p < 0.05$) in the CNS. TLR7, TLR8 and TLR9 mRNA levels, however, reached maximum at later time points. NSV infection upregulated TLR7 transcription by approximately 15-fold at 7 dpi, while TE only induced TLR7 mRNA level by 5-fold ($p < 0.05$). Although no significant difference was observed in TLR8 and TLR9 transcript levels induced by NSV and TE, these results indicated the general trends of higher upregulation of endosomal TLR genes by the more virulent NSV strain.

A

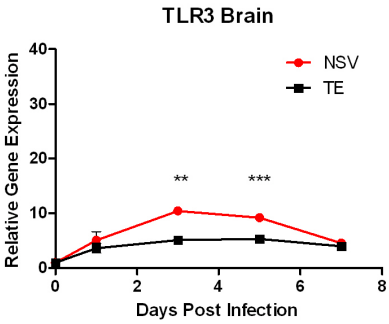
TLR3 Brain
NSV
TE
Relative Gene Expression
Days Post Infection
**
***

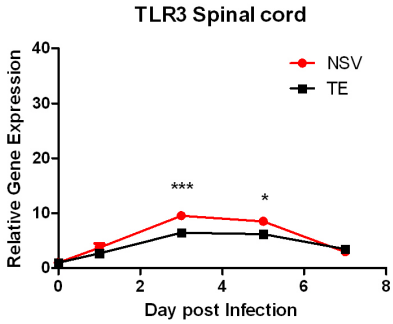
TLR3 Spinal cord
NSV
TE
Relative Gene Expression
Day post Infection
***
*

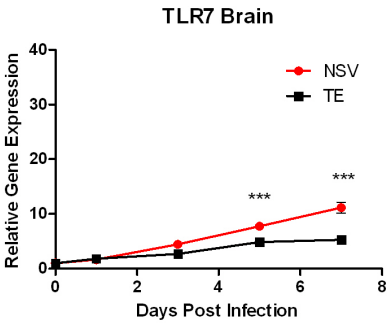
TLR7 Brain
NSV
TE
Relative Gene Expression
Days Post Infection
***
***

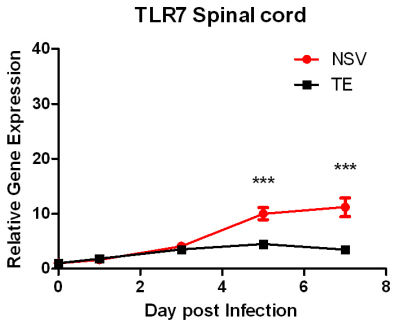
TLR7 Spinal cord
NSV
TE
Relative Gene Expression
Day post Infection
***
***

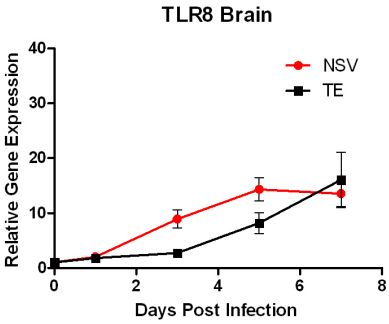
TLR8 Brain
NSV
TE
Relative Gene Expression
Days Post Infection

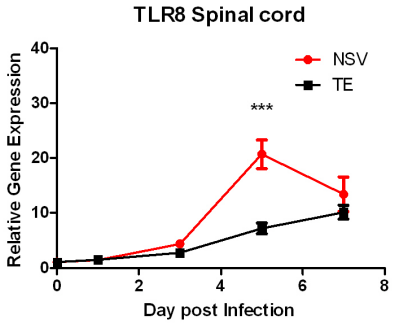
TLR8 Spinal cord
NSV
TE
Relative Gene Expression
Day post Infection
***

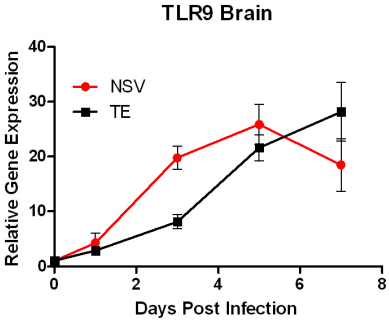
TLR9 Brain
NSV
TE
Relative Gene Expression
Days Post Infection

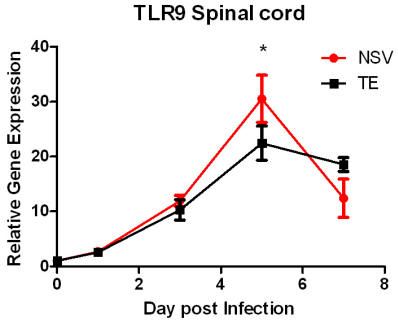
TLR9 Spinal cord
NSV
TE
Relative Gene Expression
Day post Infection
*

B

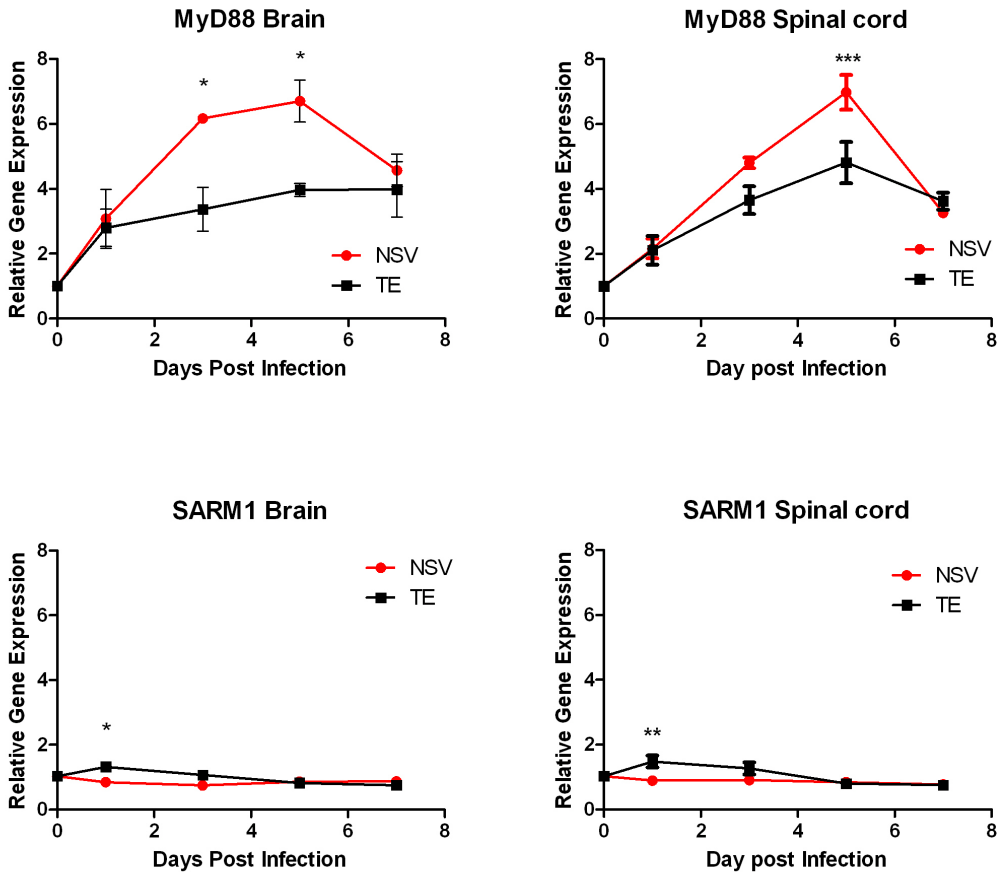

Figure 5. Upregulation of endosomal TLRs and Myd88 during SINV infection in the brain and spinal cord of wild-type mice. Wild-type adult C57BL/6 mice were intracerebrally infected with either TE or NSV strain of SINV, and RNA was extracted from the brain and spinal cord harvested at 0, 1, 3, 5 and 7 dpi. Relative gene expression of endosomal TLR3, 7, 8 and 9 (A) and TIR family adaptors MyD88 and SARM1 (B) were analyzed by semi-quantitative RT-PCR assay. The data were normalized to GAPDH mRNA levels and were expressed as the relative fold change over normalized mRNA from uninfected mice (mean ± SE). Five to six animals were included per time point for each virus strain. Two-way ANOVA with Bonferroni posttest was conducted for statistical analysis. (* $p < 0.05$, ** $p < 0.01$, *** $p < 0.001$).

Recognition of viral RNA by TLRs results in activation of TIR domain-containing adaptors MyD88 and TRIF that induce downstream signaling pathways. The fifth TIR adaptor, SARM1 is recently demonstrated to play important roles in regulating neuronal morphology and functions. TLR7/9 or MAVS-mediated SARM1 activation is also implicated in neurodegeneration. Expression levels of SARM1 and the classical TIR adaptor MyD88 were evaluated following infection with either NSV or TE strain of SINV. In the brain and spinal cord, MyD88 was upregulated by more than 6 fold and 3 fold after 3 dpi by NSV and TE as

compared to the control (Figure 5B). However, despite a mild decrease at early time points following NSV infection, SARM1 mRNA levels remained constant in the CNS.

These results showed that endosomal TLRs and MyD88 rather than SARM1 were transcriptionally upregulated in response to SINV infection. However, whether these genes were also induced at protein levels was unknown. Besides, the neurovirulent NSV strain induced higher levels of TLR3, TLR7 and MyD88 transcripts in the CNS than the TE strain of SINV. These results lead to the hypothesis that TLR-MyD88 signaling correlates with the severity of SINV-induced encephalomyelitis.

Endosomal TLRs and MyD88 are upregulated by SINV in IRF7$^{-/-}$ and IRF3$^{-/-}$ mice

IRF3$^{-/-}$ and IRF7$^{-/-}$ mice developed more severe disease after infection with the TE strain of SINV than wild type mice. IRF7$^{-/-}$ mice developed hindlimb paralysis and showed increased mortality compared to wild type or IRF3 knockout mice. To evaluate whether mRNA levels of endosomal TLRs and the downstream adaptor proteins were also upregulated in IRF3$^{-/-}$ and IRF7$^{-/-}$ mice, wild type and IRF knockout mice were infected with TE and brain and spinal cord samples were harvested at 0, 1, 3, 5, 7 dpi. RT-PCR analysis showed that TE infection significantly induced endosomal TLRs and MyD88 transcription after 3 dpi (Figure 6). Greater upregulation of the TLR and MyD88 transcripts in the brain and spinal cord was observed in IRF deficient mice compared to the wild type mice, particularly from 5 to 7 dpi. Moreover, relative changes in TLR7 mRNA levels were significantly higher in the brains of IRF7$^{-/-}$ mice compared to IRF3$^{-/-}$ mice at 5 and 7 dpi ($p < 0.001$). In the spinal cord, TLR7 mRNA was increased by an average of 14 fold in IRF7$^{-/-}$ and 10 fold in IRF3$^{-/-}$ mice (Figure 6A). As observed in TE or NSV infected wild type mice, SARM1 mRNA expression was also not prominently affected in IRF7$^{-/-}$ and IRF3$^{-/-}$ mice following TE inoculation (Figure 6B). These data implied that TLR7 might be involved in SINV pathogenesis in IRF7$^{-/-}$ mice.

A

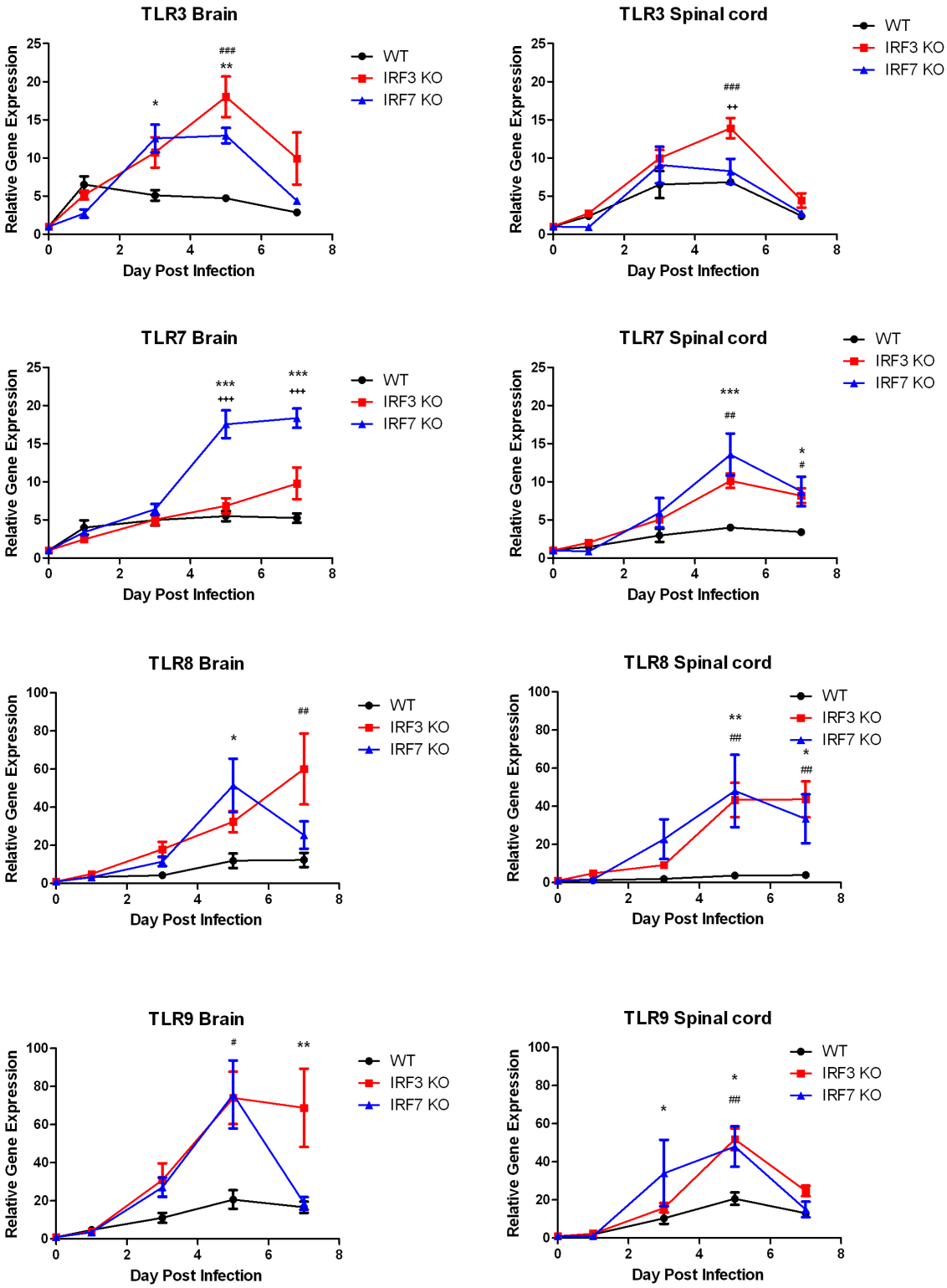
TLR3 Brain
TLR3 Spinal cord
TLR7 Brain
TLR7 Spinal cord
TLR8 Brain
TLR8 Spinal cord
TLR9 Brain
TLR9 Spinal cord
Relative Gene Expression
Day Post Infection
WT
IRF3 KO
IRF7 KO

B

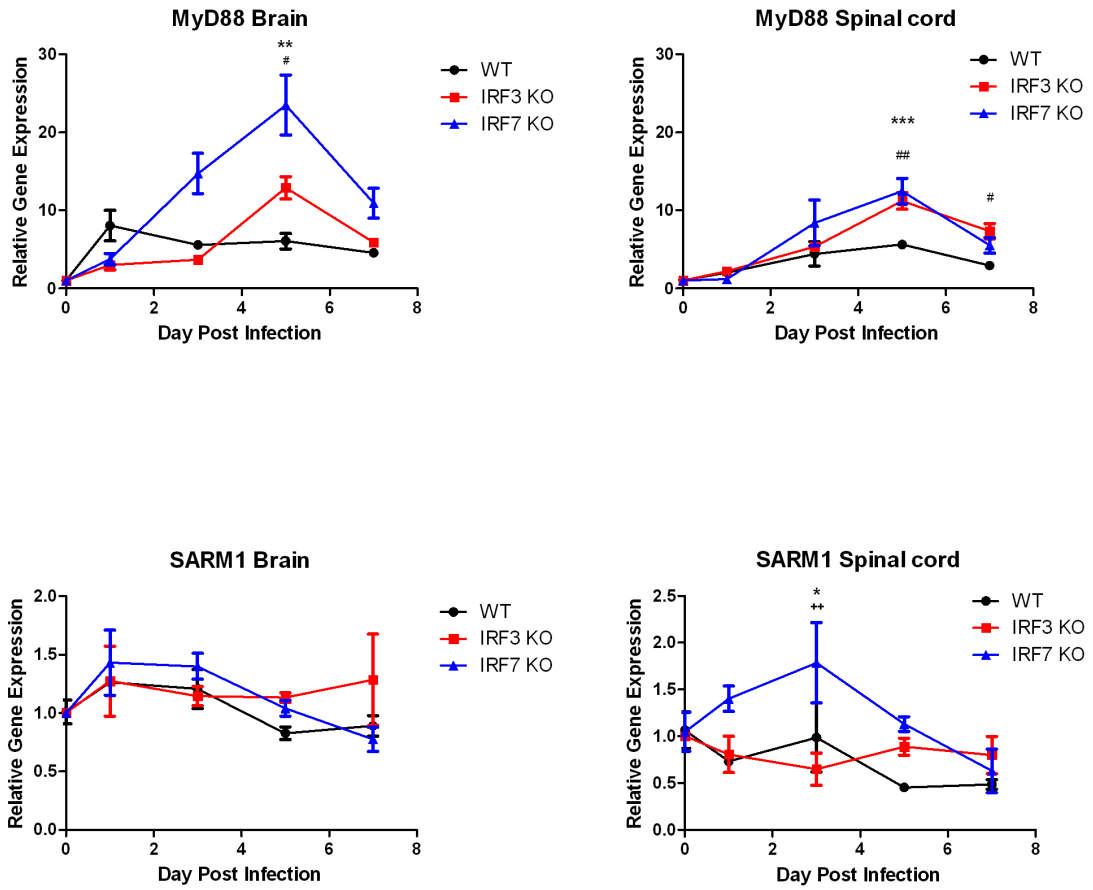

Figure 6. Upregulation of endosomal TLRs and Myd88 during SINV infection in the brain and spinal cord of wild-type and IRF knockout mice. Wild type, IRF3$^{-/-}$ and IRF7$^{-/-}$ adult C57BL/6 mice were intracerebrally infected with the TE strain of SINV, and RNA was extracted from the brain and spinal cord harvested at 0, 1, 3, 5 and 7 dpi. Relative gene expression of endosomal TLR3, 7, 8 and 9 (A) and TIR family adaptors MyD88 and SARM1 (B) were analyzed by semi-quantitative RT-PCR assay. The data were normalized to GAPDH mRNA levels and were expressed as the relative fold change over normalized mRNA from uninfected mice (mean ± SE). Five to six animals were included per time point for each mouse strain. Two-way ANOVA was conducted for statistical analysis. (* $p < 0.05$, ** $p < 0.01$, *** $p < 0.001$ represented significant difference between IRF7$^{-/-}$ and wild type mice; $^{\#}$ $p < 0.05$, $^{\#\#}$ $p < 0.01$, $^{\#\#\#}$ $p < 0.001$ represented difference between IRF3$^{-/-}$ and wild type mice; $^{+}$ $p < 0.05$, $^{++}$ $p < 0.01$, $^{+++}$ $p < 0.001$ represented difference between IRF7$^{-/-}$ and IRF3$^{-/-}$ mice).

SINV infection induces miRNA-21 and miR-146 expression in the CNS

Dysregulation of miRNAs was examined using a limited microRNA microarray analysis previously. Two miRNAs, miRNA-21a-5p and miRNA-146a-5p, were significantly induced in the brains of mice infected with TE at 5 dpi, according to the criterion of more than 2 fold upregulation. We sought to validate the expression changes of these two miRNAs by microRNA RT-PCR assay. Additionally, we would examine the dynamics of miR-21a and miR-146a expression following infection with both NSV and TE strains of SINV in the CNS. Another miRNA, let-7c-5p, was chosen as the endogenous control because of its stability and low variability on the miRNA microarrays. The relatively constant expression of let-7c-5p in the brain and spinal cord during the 7-day period of infection was confirmed by miRNA RT-PCR (Figure 7A); consequently let-7c was used for normalizing the levels of other miRNAs. In agreement with the microarray data, RT-PCR analysis revealed that miR-21a and miR-146a were significantly induced by SINV infection at 5 dpi (Figure 7B). Both miRNAs were upregulated gradually from 3 dpi in the brain and spinal cord, when compared with uninfected animals. Additionally, the neurovirulent strain NSV induced higher levels of miR-21a-5p than the less virulent TE strain; with around 10-fold increase in the brains of NSV infected mice and 5-fold increase in TE infected mice at 7 dpi (p value < 0.001). SINV-induced overexpression of miR-146a-5p was also observed in the CNS but with lower levels of change. Besides, there is little or no difference in miR-146a expression observed in NSV and TE infected brain and spinal cord (Figure 7B).

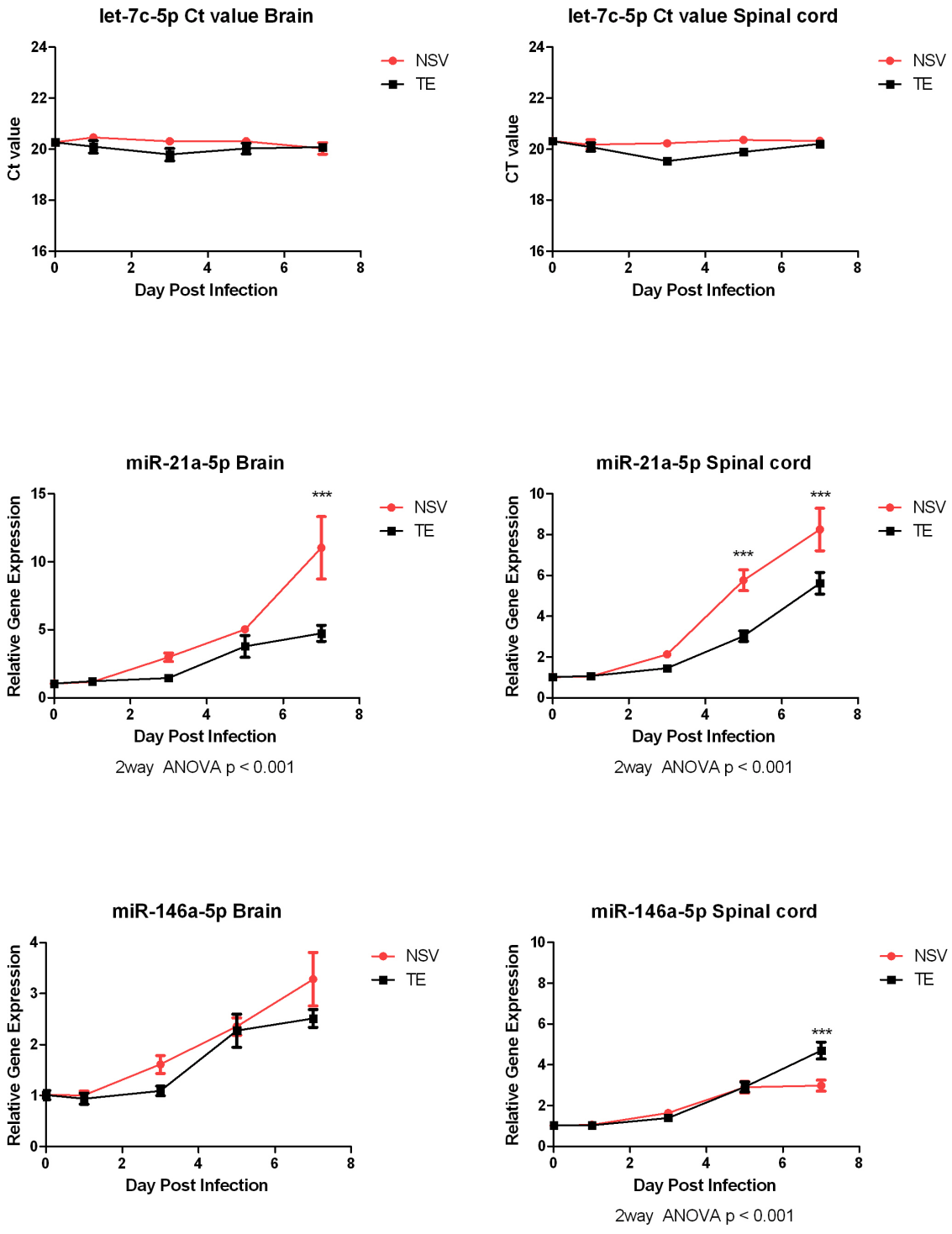

Figure 7. Induction of miR-21a and miR-146a by SINV infection in the CNS of wild type mice. Total RNA was extracted from the brain and spinal cord of wild-type adult C57BL/6 mice infected with NSV and TE for 0, 1, 3, 5 and 7 days. MicroRNA RT-PCR analysis confirmed the relative stable Ct values of let-7c in the CNS (A). Levels of miR-21a and miR-146a were normalized to endogenous let-7c levels, and relative expression changes were determined using the $2^{-\Delta\Delta Ct}$ formula (B). Experiments were run in duplicate and five to six samples were included per time point per group. Two-way ANOVA was used for statistical analysis (*** $p < 0.001$).

Because miR-146a expression was not differentially regulated in response to TE and NSV infection, we next examined only the levels of miRNA-21a expression in IRF3$^{-/-}$ and IRF7$^{-/-}$ mice. Consistent with the results in wild type mice, miRNA RT-PCR revealed that miR-21a was also significantly induced by TE infection in IRF knockout mice compared with uninfected controls (Figure 8). Additionally, higher levels of miR-21a were present in both IRF3$^{-/-}$ and IRF7$^{-/-}$ mice, with approximately 8-fold increase in knockout mice and 4-fold increase in wild type mice at 7 dpi (p value < 0.001, Figure 8). These results indicated that miR-21 dysregulation might correlate with the severity of SINV-induced encephalitis.

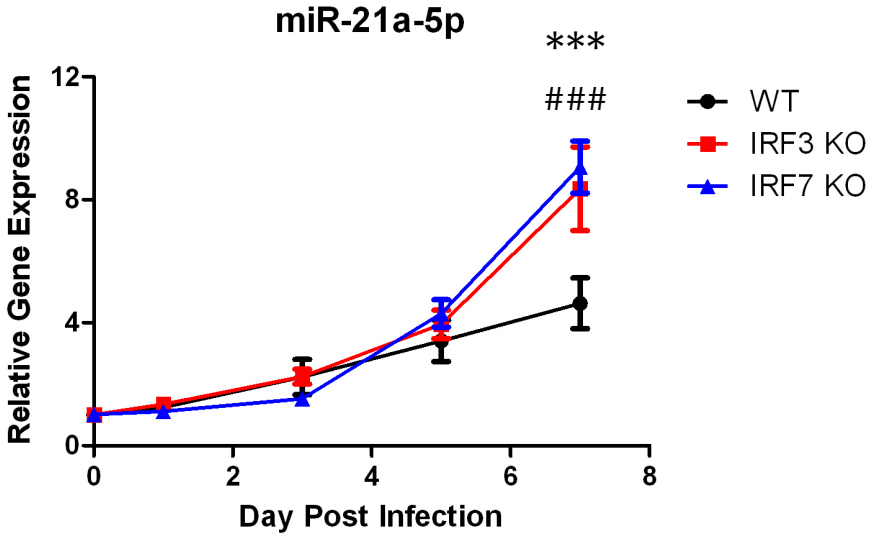

Figure 8. miR-21a upregulation by SINV in the brain of wild-type and IRF knockout mice. Total RNA was extracted from the brain wild type, IRF3$^{-/-}$ and IRF7$^{-/-}$ C57BL/6 mice infected with TE strain of SINV. MicroRNA RT-PCR analysis was performed to determine the relative expression levels of miR-21a after 0, 1, 3, 5 and 7 dpi. Data were normalized to endogenous let-7c levels, and relative expression changes were calculated using the $2^{-\Delta\Delta Ct}$ formula. Experiments were run in duplicate and three samples were included per time point per group. Two-way ANOVA with Bonferroni post-hoc test was used for statistical analysis (*** $p < 0.001$ indicated significant difference between IRF7$^{-/-}$ and wild type mice; $^{###}$ $p < 0.001$ indicated difference between IRF3$^{-/-}$ and wild type mice).

NSC34 cells were not fully differentiated

Owing to their motor neuron origin, NSC34 cell line is commonly employed as an *in vitro* system for studying motor neuron diseases such as amyotrophic lateral sclerosis (ALS) and traumic spinal cord injury (SCI). As SINV infection induces differential cell death mechanisms in neurons from different sources, we investigated the mechanisms of SINV-induced motor neuron degeneration using the NSC34 cell line. To better mimic motor neurons in adult mice, NSC34 cells were differentiated by serum depletion and addition of 10 μM *all-trans* retinoic acid (*at*RA). This is higher than the concentration of 1 μM previously reported in the literature, possibly due to variation of origin and repeated passage of the cell line. NSC34 cells grown in *at*RA-containing differentiation medium for more than 2 days displayed inhibited cell proliferation and significant neurite outgrowth (Figure 9A). The phenotype of differentiated motor neurons, however, started to disappear after one week, suggesting the incomplete differentiation of NSC34 cells under this condition. Culturing cells on matrigel-coated plates accelerated cell differentiation, but was also unable to help maintain the differentiated state.

Resistance to SINV infection increased with NSC34 maturation (Figure 9B). However, consistent with previous results, these partially differentiated NSC34 cells remained permissive to SINV. Unlike differentiated AP7 (a rat odora olfactory neuronal cell line) and CSM14.1 (a rat mesencephalic progenitor cell line) that are able to restrict virus replication, 4 day differentiated NSC34 cells replicated TE strain of SINV to comparable titers as undifferentiated NSC34 cells by 48 hpi (Figure 9B) [15]. Therefore, whether differentiated NSC34 cells represents a suitable *in vitro* model for studying SINV-induced motor neuron necrotic cell death in adult mice spinal cord is questionable.

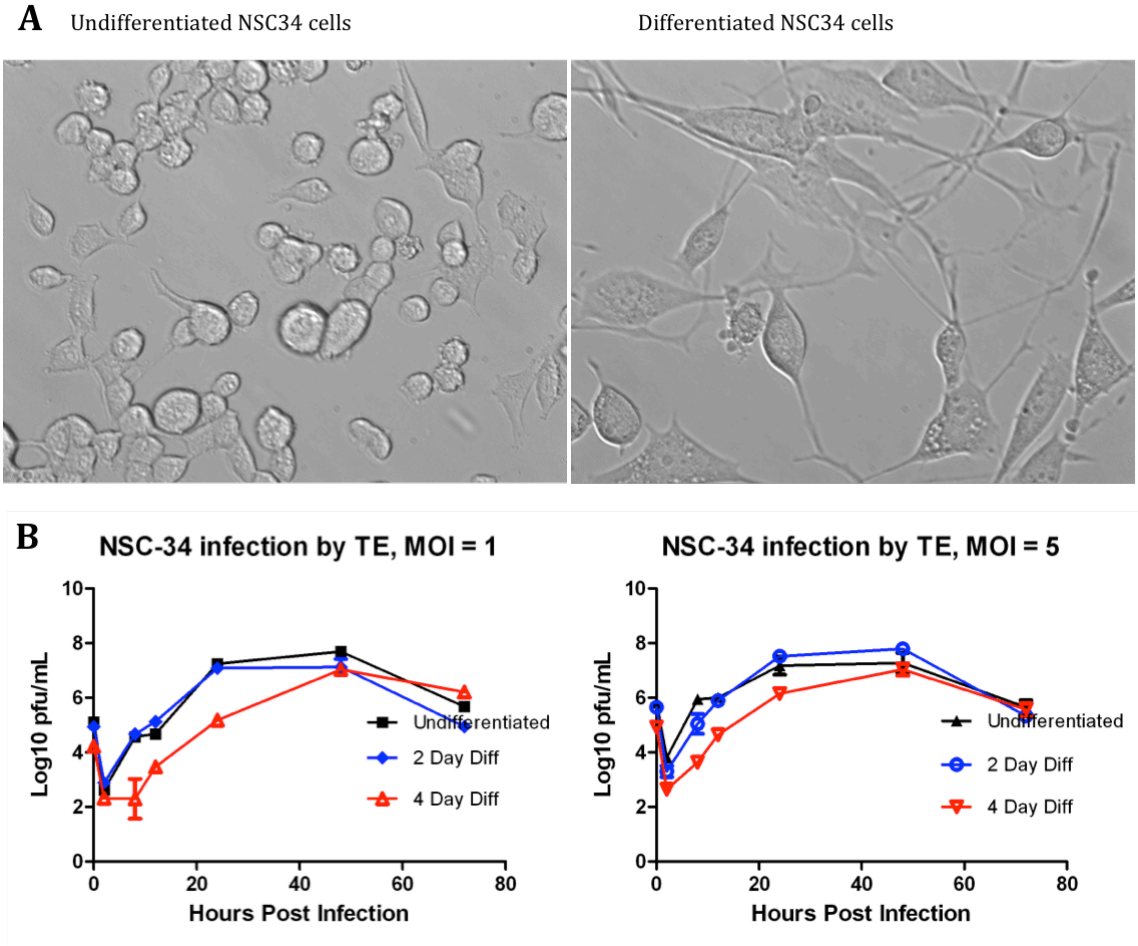

Figure 9. Morphology and SINV growth curves in cycling and differentiated NSC-34 cells. Undifferentiated cells had short or no neurites, while extensive neuron-like processes were observed in NSC34 cells cultured in differentiation medium with 1% FBS and 10 µM *at*RA. Representative images of undifferentiated and 3 day differentiated cells were captured using phase contrast microscope (20x magnification) (A). Cycling, 2 day- and 4 day-differentiated NSC34 cells were infected with the TE strain of SINV at an MOI of 1 or 5. Viral titers in supernatant fluids of TE infected NSC34 cells were determined using plaque assay on BHK cells over 72 hours post infection (B). Results were expressed as the average log10 pfu/ ml ± standard error of three different wells.

RIP3 expression is undetectable in NSC34 cells

RIP3 is a crucial regulator of necroptotic cell death. Elevated RIP3 expression is an indicative marker for this regulated necrosis pathway and has been observed in damaged tissue in various disease models such as alcoholic liver disease, inflammatory bowel disease, ischemic brain/ spinal cord injury and ALS. To assess the involvement of necroptosis in SINV-induced neuronal cell death, we investigated the expression of RIP3 protein in NSC34 cells using western blotting. The anti-RIP3 antibody detected a band of about 57 kDa, demonstrated in the small intestine samples that served as positive controls. We were unable to observe endogenous RIP3 protein in either undifferentiated or 4 day-differentiated NSC34 cells (Figure 10). In addition, TE strain of SINV infection at an MOI of 1 in cycling and differentiated NSC34 cells also did not induce detectable levels of RIP3.

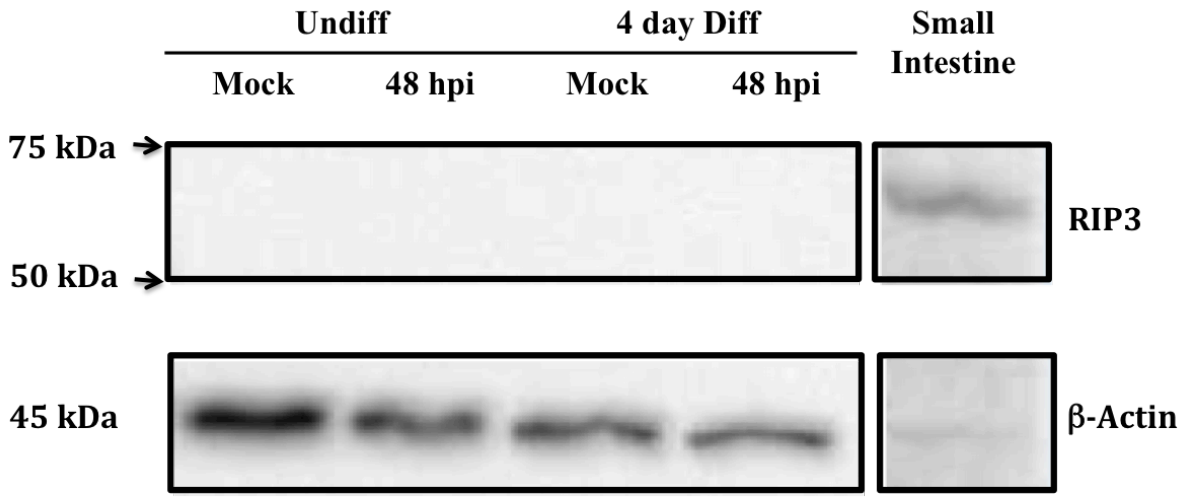

Figure 10. Western blot analysis of RIP3 in NSC34 cells infected with SINV. Undifferentiated and 4 day-differentiated NSC34 cells were infected with TE strain of SINV at an MOI of 1. Mock or TE infected NSC34 cells were collected at 48 hpi. Protein lysates were resolved by SDS-PAGE and analyzed by western blotting using a rabbit monoclonal anti-RIP3 antibody (Cell signaling, Cat. no. 95702S). No bands were detected within the estimated range of 46-62 kDa. Extracts of mice small intestine was loaded as a positive control.

SINV infection does not induce RIP3 overexpression in the spinal cord

Necroptosis drives motor neuron degeneration in ALS and spinal cord injury. To evaluate whether NSV-induced motor neuron necrosis is necroptotic, we first investigated the changes in RIP3 and MLKL mRNA levels in the brain and spinal cord following SINV infection. Semi-quantitative RT-PCR showed that RIP3 and MLKL mRNA levels were upregulated by the TE and NSV strains of SINV virus in both brain and spinal cord over time with relatively higher expression levels induced by the NSV strain (Figure 11). RIP3 mRNA expression was significantly higher at 7 dpi in the brain ($p < 0.001$) and at 5 dpi in the spinal cord ($p < 0.01$) in NSV infected mice compared to the TE group. The average MLKL transcription levels were also higher in the brain and spinal cord of NSV infected mice compared with TE infected ones, although no significant differences were observed. Besides, greater relative change in RIP3 and MLKL expression occurred in the brain rather than in the spinal cord. For instance, NSV infection increased RIP3 mRNA by approximately 33-fold in the brain and 23-fold in the spinal cord at 7 dpi; MLKL mRNA levels peaked at 5 dpi following NSV infection, with roughly 129-fold increase in the brain and 61-fold in the spinal cord.

We then compared RIP3 protein levels in the spinal cords of mice infected with TE and NSV. We intracerebrally infected C57BL/6 mice with either TE or NSV strain of SINV, and collected spinal cord samples, at 5 and 7 dpi when motor neuron necrosis was likely to occur. Western blot analysis showed that RIP3 was expressed at very low levels in the CNS compared to other tissues [67]. As in Figure 12A, the 57 kDa bands were faint when 150 μg of protein from spinal cords was loaded. By contrast, darker bands were detected when only 40 μg protein from small intestine homogenates were resolved. Expression levels of RIP3 protein were highly variable in each group, and no significant increase in RIP3 expression was detected in the spinal cords of TE or NSV infected mice compared to the uninfected group (Figure 12B). Therefore, western blotting could not provide any conclusive evidence to show SINV infection induce RIP3 upregulation or necroptotic cell death in the spinal cords.

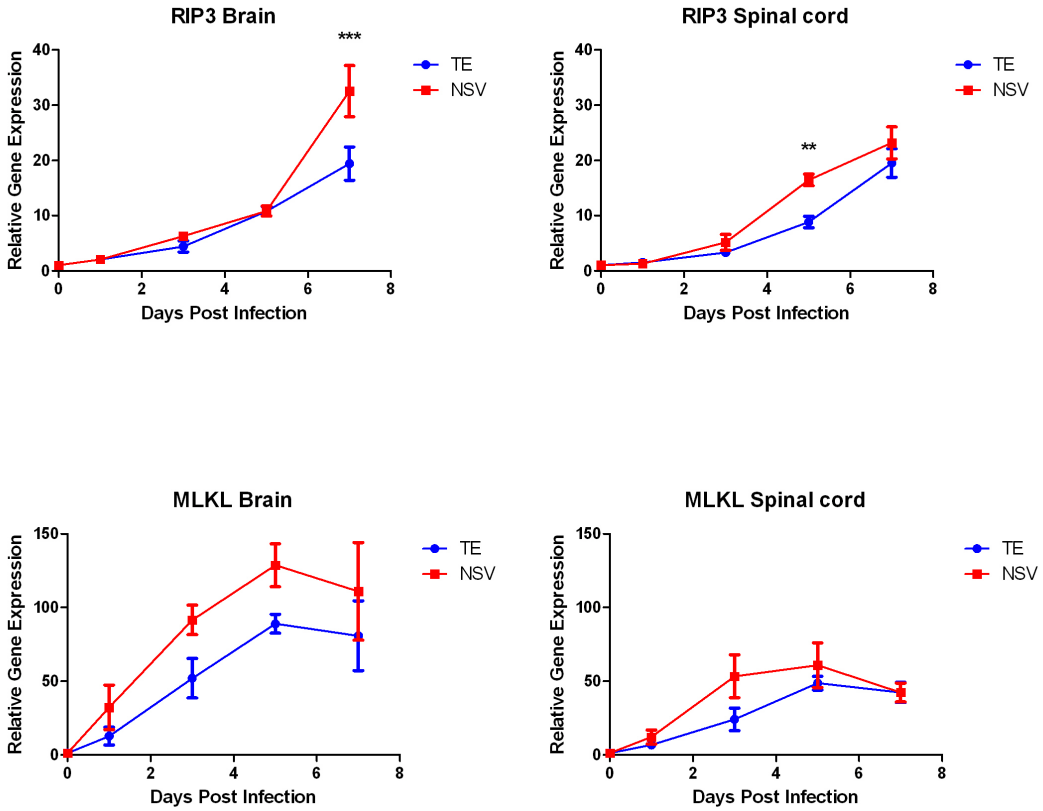

Figure 11. RIP3 and MLKL mRNAs are upregulated during SINV infection in the brain and spinal cord of wild-type mice. Wild-type adult C57BL/6 mice were intracerebrally infected with either TE or NSV strain of SINV, and RNA was extracted from the brain and spinal cord harvested at 0, 1, 3, 5 and 7 dpi. Relative gene expression of RIP3 and MLKL mRNAs were analyzed by semi-quantitative RT-PCR assay. The data were normalized to endogenous GAPDH mRNA levels and were expressed as the relative fold change over normalized mRNA from uninfected mice (mean ± SE). Five to six animals were included per time point for each virus strain. Two-way ANOVA with Bonferroni posttest was conducted for statistical analysis. (** $p < 0.01$, *** $p < 0.001$).

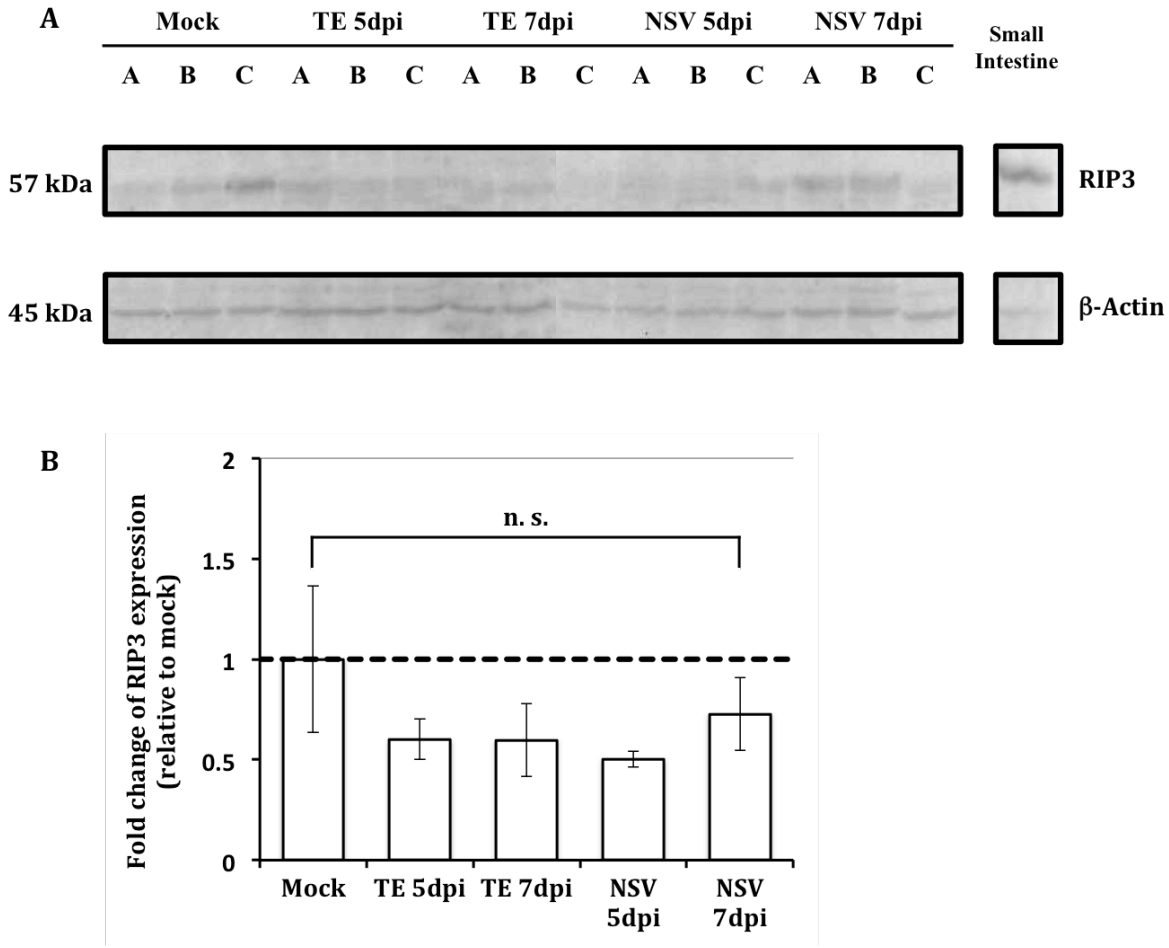

Figure 12. Western blot analysis of RIP3 expression in the spinal cord following SINV infection. Wild-type C57BL/6 mice were intracerebrally infected with either TE or NSV strain of SINV at four to six weeks of age. Spinal cords were harvested at 0 (mock), 5 and 7 dpi and homogenized in RIPA buffer. Protein lysates were resolved by SDS-PAGE and analyzed by western blotting using a rabbit monoclonal anti-RIP3 antibody (Cell signaling, Cat. no. 95702S) (A). To confirm the specificity of the anti-RIP3 antibody, extracts of small intestine from uninfected C57BL/6 mice was loaded as a positive control. The intensities of protein bands were quantified using the NIH ImageJ software (http://rsbweb.nih.gov/ij/) and the loading differences were normalized with reference to the -actin bands. Densitometric analysis from three independent samples showed no statistical difference between RIP3 expression levels in TE or NSV infected mice spinal cords and those in uninfected controls (B). Two-way ANOVA with Bonferroni posttests was used for statistical analysis.

Next we examined RIP3 protein expression in the spinal cord using immunohistochemistry staining. Since the slides from the NSV infected wild type mice were presently not available, I evaluated RIP3 protein levels in the spinal cord of wild type, IRF3-/- and IRF7-/- adult C57BL/6 mice instead. As TE infection also induces caspase-3 independent neuronal death in the spinal cord and causes hindlimb paralysis in $IRF7^{-/-}$ mice like the NSV strain did in wild type mice, we hypothesized that motor neuron degeneration in these two cases involves the same cell death mechanism. Wild type, $IRF3^{-/-}$ and $IRF7^{-/-}$ adult C57BL/6 mice were intracerebrally infected with the TE strain of SINV, and the spinal cord samples were obtained at 5 and 7 dpi. Immunohistochemical analysis was performed using anti-RIP3 antibody (Abcam ab56164), and no RIP3 positive cell was detected in the spinal cord sections of all three strains of mice at 5 or 7 dpi. Representative figures of 7 dpi sections were shown in Figure 13 A-C. To confirm the immunoreactivity of this antibody, the same procedures were performed with small intestine and stomach sections obtained from wild type, uninfected mice. As in Figure 13D, RIP3 expression was detected in gastric mucosa lamina, which is consistent with the literature [67]. These suggested that infection with the TE strain of SINV did not induce RIP3 expression detectable by immunohistochemistry in the spinal cord of $IRF^{-/-}$ mice.

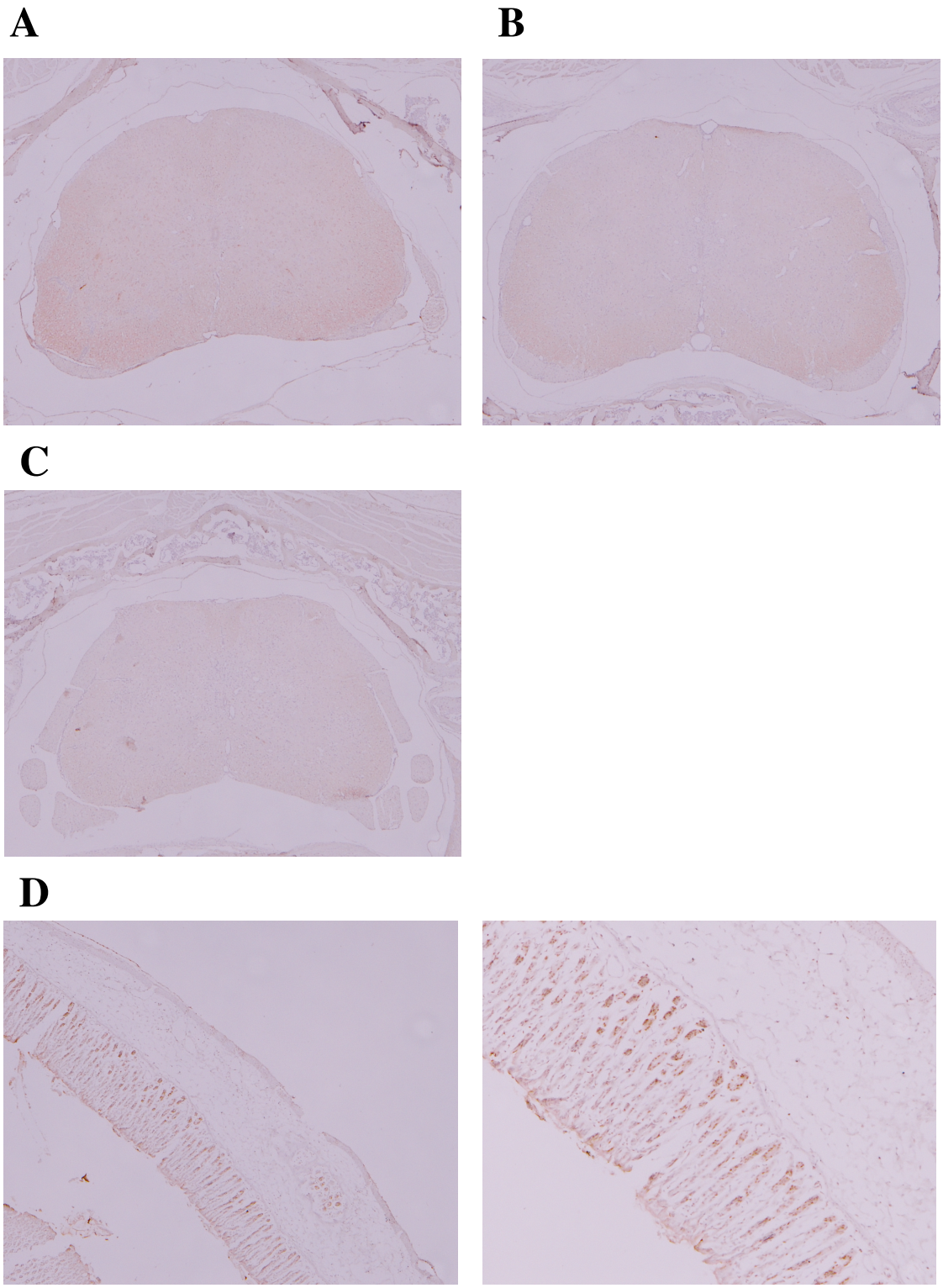

Figure 13. Immunohistochemistry analysis of RIP3 expression in the spinal cord following SINV infection. Wild type, IRF3$^{-/-}$ and IRF7$^{-/-}$ adult C57BL/6 mice were intracerebrally infected with the TE strain of SINV, and the spinal cord samples were obtained harvested at 7 dpi. Representative pictures of immunostaining for RIP3 in the spinal cord of wild type (A), IRF3$^{-/-}$ (B) and IRF7$^{-/-}$ (C) are shown. A photo of RIP3 staining in the stomach serves as the positive control (D). The arrow indicates RIP3-positive cell. Original magnification × 4, magnification × 10 for area of interest in the stomach.

Discussion

TLR signaling and SINV infection

The adaptive immune response plays critical roles in the pathogenesis of SINV-induced encephalomyelitis, yet the roles of innate immune pathways in regulating these processes have not been clarified. Endosomal TLRs are known to detect viral nucleic acids or replication complexes, and thus are considered central to immune defense against viral infections. Recent studies also showed that endosomal TLR activation in neurons can induce neuronal apoptosis or necroptosis, in an MyD88-dependent or SARM1-dependent manner. The fifth member of TIR family adaptor protein, SARM1, is abundantly expressed in neurons and has been implicated in neuronal cell death triggered by oxygen glucose deprivation, mitochondria dysfunction and viral infection. Using RT-PCR, we observed that all four endosomal TLRs selected for analysis and MyD88 were upregulated in the brain and spinal cord following SINV infection at a transcriptional level. In addition, the level of induction seemed to correlate with the severity of symptoms. The fatal NSV strain of SINV stimulated higher levels of TLR3, TLR7 and MyD88 mRNAs than the TE strain in the CNS. TLR7 mRNA levels were also significantly higher in TE infected IRF7$^{-/-}$ mice than in IRF3$^{-/-}$ and wild type mice, which were relatively less susceptible to SINV infection.

Although we did not investigate the expression of endosomal TLRs and associated adaptors at the protein levels, these findings provided preliminary data suggesting that endosomally located TLRs, especially TLR7, might be involved in SINV pathogenesis. However, one study has shown that survival from NSV encephalitis in MyD88 and TLR3 knockout mice was not significantly different from wild type mice [68]. This conflicts with our hypothesis that TLR-dependent signaling contributes to SINV disease outcome. Nevertheless, TLR3 and MyD88 mediated pathways may have redundant functions. Another possibility is SINV may activate endosomal TLR signaling that requires a noncanonical adaptor protein, for instance SARM1, rather than the classical MyD88 protein.

SARM1 mRNA expression was not affected by SINV infection in the brain and spinal cord. Nonetheless, we cannot rule out the possibility that SARM1 is regulated at the posttranscriptional level. For example, the TLR4 ligand LPS was previously reported to induce a rapid increase in SARM1 protein without affecting mRNA expression. Intracellular localization and dimerization are also important determinants for the functions of this adaptor protein. For instance, Mukherjee *et al*. demonstrated SARM1 trafficking and accumulation in mitochondria during TLR7/ 9 stimulation-induced apoptosis in primary cortical neurons [24]. However, SARM1 translocation to the nucleus was reported to inhibit TNF induced apoptosis of HEK293 cells [69]. Besides, SARM1 dimerization through TIR domain interaction in response to neuronal injury triggers rapid consumption of NAD+ and decline in ATP level which leads to neuronal cell death or local axonal degeneration [70]. Further studies will be necessary to determine the roles of endosomal TLR- SARM1 signaling during SINV pathogenesis [30].

MiRNAs are small non-coding RNAs that typically bind to 3' untranslated regions of mRNA and thus mediate posttranscriptional gene regulation. Recent studies demonstrate that miRNAs are capable of regulating virus-host interactions. Several DNA viruses and retroviruses, such as herpesviruses, encode viral miRNAs that can regulate both viral and host gene expression. Additionally, virus infections have been reported to alter the cellular miRNA expression profile. Viruses can hijack the cellular miRNA machinery to regulate their own replication, translation and pathogenesis, either by directly interacting with cellular miRNAs or by indirectly modulating host miRNA synthesis [71, 72].

Here, we validated the results of previous microRNA microarray data from Dr. Yoshinari Ando that suggested upregulation of miR-21 and miR-146 in the brain and spinal cord during SINV infection by more than 2-fold. MicroRNA RT-PCR analysis showed that both miRNAs steadily accumulated during 7 dpi. Moreover, significantly higher levels of miR-21 were observed in NSV-infected wild type mice than those infected by the TE strain, and in the brains of TE-infected IRF deficient mice than those of wild type mice. However, the

mechanism, localization and functional relevance of this differential regulation are still not clear. MiR-21 is a well-studied "onco-miRNA" in tumor cells that regulate cell growth, migration, invasion and apoptosis through the suppression of its target genes such as BCL-2 and Programmed cell death 4 (PDCD4). In neurons, miR-21 is reported to repress a CNS transcription factor, myocyte enhancer factor 2C (MEF2C), which is crucial for neuronal survival and functions [31]. Besides, miR-21 also modulates the production of type I IFNs and ISGs by targeting MyD88 and IRAK1 in the TLR signaling pathway. Several viruses including HCV, HIV and VSV upregulate miR-21, suppress antiviral immune response and promote virus replication [72]. Furthermore, miR-21 contains specific GU-rich motif that can directly bind and activate TLR7 signaling pathway. Yelamanchili *et al*. recently demonstrated that endogenous miR-21 was enriched in macrophage-derived EVs and induced a novel neurotoxic signaling pathway via neuronal TLR7 in SIV encephalitic brains [30]. Increased expression of EV miR-146 was also reported in mouse models of TBI and SIV encephalitis [73]. This miRNA can be activated by proinflammatory stimuli such as LPS and was considered to control inflammation in a negative feedback loop [74, 75]. MiR-146 in EVs was shown to downregulate IRAK1 and TRAF6 that were involved in TLR signaling cascades in recipient cells [74, 75].

Therefore, the mRNA and miRNA RT-PCR analysis here suggested that SINV infection activated transcriptional upregulation of endosomal TLRs, MyD88, miR-21 and-146 in the brain and spinal cord. The degree of upregulation of these genes, particularly TLR7 and miR-21, appeared to correlate with the severity of encephalitic disease. At this point, it remains unclear whether SINV activates miR-21-TLR7 mediated neurotoxicity pathway like SIV.

Regulated necrosis and SINV infection

Previous studies in our lab showed that the NSV strain of SINV activates divergent neuronal cell death pathways in the brain and spinal cord. Unlike NSV-induced apoptotic neurons in the brain of infected animals, damaged motor neurons display morphologic and biochemical characteristics of necrotic cells. Recent evidence indicates that necrosis can be a genetically programmed event and multiple forms of regulated necrosis have been described based on their unique molecular machinery. These include necroptosis, pyroptosis, parthanatos, oxytosis, ferroptosis and several other modes of cell death [44-46].

Necroptosis is the most extensively studied programmed necrosis pathway and can be activated by a variety of stimuli such as TNF, Fas ligand, TLR3/ 4 agonists and DAI ligands [36]. Necroptosis is an inflammatory form of cell death and has been implicated in motor neuron degeneration in ALS and traumatic spinal cord injury. Earlier work demonstrates that increased secretion of TNF, the classical necroptosis agonist, is induced by SINV infection both *in vitro* and *in vivo* [64, 66]. TNFα and TNFR deficiency are also reported to protect mice from fatal NSV diseases [65, 66]. Therefore, we proposed that TNF or PRRs- triggered necroptosis might contribute to SINV pathogenesis in motor neurons.

To investigate the hypothesis that necroptosis drives SINV-induced motor neuron loss, we first examined the regulation of RIP3 and MLKL mRNA in the brain and spinal cord in response to SINV infection. We showed that both RIP3 and MLKL were upregulated at a transcriptional level and the fatal NSV strain induced a greater change relative to the TE strain. However, more prominent upregulation was observed in the brain compared to the spinal cord for both genes, which can be conflicting with our original hypothesis that RIP3-mediated necroptosis contributed to SINV-induced motor neuron degeneration.

Then we assessed the expression of RIP3 protein in the spinal cord during SINV encephalomyelitis. However, we did not find any evidence of RIP3 upregulation in response to SINV infection using either western blotting or immunohistochemical staining. Western

blots showed that neither NSV nor TE strain of SINV promoted significantly increased levels of RIP3 in the spinal cord lysates relative to the uninfected controls, at 5 and 7 dpi when mice develop hindlimb paralysis. Owing to the low RIP3 expression levels and high background of the western blots, the aforementioned results were questionable. RIP3 protein was also undetectable by immunohistochemistry staining in the spinal cord of TE infected IRF7$^{-/-}$ mice, in which similar caspase-3 independent necrotic cell death was observed. Consistent with previous reports, both western blot and immunohistochemistry analysis showed that RIP3 protein levels in the CNS were much lower than in other tissues, such as small intestine and stomach that served as positive controls [67]. Therefore, RIP3 protein was not induced to a detectable level in the spinal cord, though transcriptional upregulation was observed.

Protein levels of RIP3 were also measured in SINV-infected NSC34 cells using western blotting. No RIP3 expression was observed above background levels in the homogenates of immature or 4-day differentiated NSC34 cells. In addition, we also failed to detect RIP3 protein during the 48 hours post TE infection, though this might be attributable to the small amount of total protein resolved in the experiment. Additionally, RIP3 upregulation may occur after the 2-day period of infection included in the study; therefore, later time points should be examined in further studies. In view of the variation of cell line and incomplete differentiation, the use of differentiated NSC34 cells as *in vitro* model to study motor neuron disease is also problematic. Furthermore, majority of dead neurons in the lumbar spinal cord were not directly infected with NSV, suggesting that NSV activated a non-autonomous death pathway [78]. Consequently, co-culture motor neurons with glial cells may be more suitable for studying the cell death mechanism.

In conclusion, we are unable to generate conclusive evidence for SINV-induced necroptosis in the spinal cord at the moment. Given the technical obstacles of RIP3 measurement, other biomarkers of necroptosis ought to be considered. Besides, RIP3 upregulation alone is also inconclusive due to the functions of RIP3 beyond necroptosis, including NF□B activation, inflammasome stimulation, kinase-independent apoptosis and cell death-independent

neuroinflammation [79, 80]. Hence, combined examination of these biomarkers, including but not limited to RIP1 upregulation/ phosphorylation, RIP1-RIP3/ RIP3-MLKL interactions, MLKL upregulation/ activation/ translocation, is required to evaluate the existence of necroptosis in SINV encephalomyelitis [76]. Pharmacologic blockade with synthetic inhibitors such as necrostatin-1, GSK-872 and NSA are also useful tools for studying necroptosis [76]. Considering the relatively higher levels of RIP3 and MLKL mRNAs in the brains, it will also be interesting to explore the roles of RIP3 pathways in this region in future studies. For instance, RIP3 activation induced neuroinflammation was recently demonstrated in the model of WNV encephalitis.

Obviously, other forms of regulated necrosis can mediate SINV-induced motor neuron damage. For instance, oxytosis describes glutamate-induced oxidative cell death in neurons. In oxytosis (Figure 3), excessive extracellular glutamate can induce decreased cysteine import through the system X^{C-} Cys/Glu antiporters and increased Ca^{2+} influx, which leads to GSH depletion, GPX4 inhibition, lipoxygenases overactivation and lipid peroxidation [44, 46]. Selective ablation of GPX4 in neurons results in rapid motor neuron death and development of paralysis, suggesting that motor neurons might be more vulnerable to oxytosis [81]. Several studies suggest that glutamate excitotoxicity plays a critical role in NSV-induced motor neuron degeneration [77, 82]. Besides, reactive oxygen species accumulation and lipid peroxidation were identified in lumbar spinal cord tissues derived from NSV-infected mice within 72 hpi [82]. These suggest that oxytosis can be another potential regulated necrosis pathway that contributes to NSV-induced motor neuron death. This neuronal death can be the combined outcome of regulated or accidental necrotic pathways. Further studies would potentially elucidate the mechanisms of SINV pathology in the spinal cords.

References

1. Ludlow M, Kortekaas J, Herden C, et al. Neurotropic virus infections as the cause of immediate and delayed neuropathology. *Acta Neuropathol*. 2016;131(2):159-184.
2. Ronca SE, Dineley KT, Paessler S. Neurological sequelae resulting from encephalitic alphavirus infection. *Front Microbiol*. 2016;7:959.
3. CDC. West Nile Virus and Other Nationally Notifiable Arboviral Diseases — United States, 2015. Retrieved Feb 2017, form https://www.cdc.gov/mmwr/volumes/66/wr/mm6602a3.htm
4. Adouchief S, Smura T, Sane J, Vapalahti O, Kurkela S. Sindbis virus as a human pathogen-epidemiology, clinical picture and pathogenesis. *Rev Med Virol*. 2016;26(4):221-241.
5. Chandak NH, Kashyap RS, Kabra D, et al. Neurological complications of chikungunya virus infection. *Neurol India*. 2009;57(2):177-180.
6. Inglis FM, Lee KM, Chiu KB, et al. Neuropathogenesis of chikungunya infection: Astrogliosis and innate immune activation. *J Neurovirol*. 2016;22(2):140-148.
7. Griffin DE. Alphavirus encephalomyelitis: Mechanisms and approaches to prevention of neuronal damage. *Neurotherapeutics*. 2016;13(3):455-460.
8. ViralZone. Retrieved Feb 2017, form http://viralzone.expasy.org/all_by_species/625.html
9. Byrnes AP, Griffin DE. Binding of Sindbis virus to cell surface heparan sulfate. *J Virol* 1998;72:7349–7356.
10. Tucker PC, Lee SH, Bui N, Martinie D, Griffin DE. Amino acid changes in the Sindbis virus E2 glycoprotein that increase neurovirulence improve entry into neuroblastoma cells. *J Virol* 1997;71:6106–6112
11. Atkins GJ, Sheahan BJ. Molecular determinants of alphavirus neuropathogenesis in mice. *J Gen Virol*. 2016;97(6):1283-1296.

12. Havert MB, Schofield B, Griffin DE, Irani DN. Activation of divergent neuronal cell death pathways in different target cell populations during neuroadapted sindbis virus infection of mice. *J Virol*. 2000;74(11):5352-5356.

13. Griffin DE. Role of the immune response in age-dependent resistance of mice to encephalitis due to Sindbis virus. *J Infect Dis* 1976;133:456–464.

14. Tucker PC, Griffin DE. Mechanism of altered Sindbis virus neurovirulence associated with a single-amino-acid change in the E2 glycoprotein. *J Virol* 1991;65:1551–1557

15. Schultz KL, Vernon PS, Griffin DE. Differentiation of neurons restricts Arbovirus replication and increases expression of the alpha isoform of IRF-7. *J Virol* 2015;89:48–60.

16. Griffin DE. Viral encephalomyelitis. *PLoS Pathog*. 2011;7(3):e1002004.

17. Griffin DE. Immune responses to RNA-virus infections of the CNS. *Nat Rev Immunol*. 2003;3(6):493-502.

18. Carty M, Reinert L, Paludan SR, Bowie AG. Innate antiviral signalling in the central nervous system. *Trends Immunol*. 2014;35(2):79-87.

19. O'Neill LA, Golenbock D, Bowie AG. The history of toll-like receptors - redefining innate immunity. *Nat Rev Immunol*. 2013;13(6):453-460.

20. Carty M, Goodbody R, Schroder M, Stack J, Moynagh PN, Bowie AG. The human adaptor SARM negatively regulates adaptor protein TRIF-dependent toll-like receptor signaling. *Nat Immunol*. 2006;7(10):1074-1081.

21. Panneerselvam P, Ding JL. Beyond TLR signaling-the role of SARM in antiviral immune defense, apoptosis & development. *Int Rev Immunol*. 2015;34(5):432-444.

22. Summers DW, DiAntonio A, Milbrandt J. Mitochondrial dysfunction induces Sarm1-dependent cell death in sensory neurons. *J Neurosci*. 2014;34(28):9338-9350.

23. Veriepe J, Fossouo L, Parker JA. Neurodegeneration in C. elegans models of ALS requires TIR-1/Sarm1 immune pathway activation in neurons. *Nat Commun*. 2015;6:7319.

24. Mukherjee P, Winkler CW, Taylor KG, et al. SARM1, not MyD88, mediates TLR7/TLR9-induced apoptosis in neurons. *J Immunol*. 2015;195(10):4913-4921.

25. Mukherjee P, Woods TA, Moore RA, Peterson KE. Activation of the innate signaling molecule MAVS by bunyavirus infection upregulates the adaptor protein SARM1, leading to neuronal death. *Immunity*. 2013;38(4):705-716.

26. Hou YJ, Banerjee R, Thomas B, et al. SARM is required for neuronal injury and cytokine production in response to central nervous system viral infection. *J Immunol*. 2013;191(2):875-883.

27. Fabbri M. TLRs as miRNA receptors. *Cancer Res*. 2012;72(24):6333-6337.

28. Paschon V, Takada SH, Ikebara JM, et al. Interplay between exosomes, microRNAs and toll-like receptors in brain disorders. *Mol Neurobiol*. 2016;53(3):2016-2028.

29. Qiu L, Tan EK, Zeng L. microRNAs and neurodegenerative diseases. *Adv Exp Med Biol*. 2015;888:85-105.

30. Yelamanchili SV, Lamberty BG, Rennard DA, et al. MiR-21 in extracellular vesicles leads to neurotoxicity via TLR7 signaling in SIV neurological disease. *PLoS Pathog*. 2015;11(7):e1005032.

31. Yelamanchili SV, Chaudhuri AD, Chen LN, Xiong H, Fox HS. MicroRNA-21 dysregulates the expression of MEF2C in neurons in monkey and human SIV/HIV neurological disease. *Cell Death Dis*. 2010;1:e77.

32. Lehmann SM, Kruger C, Park B, et al. An unconventional role for miRNA: Let-7 activates toll-like receptor 7 and causes neurodegeneration. *Nat Neurosci*. 2012;15(6):827-835.

33. McKimmie CS, Johnson N, Fooks AR, Fazakerley JK. Viruses selectively upregulate toll-like receptors in the central nervous system. *Biochem Biophys Res Commun*. 2005;336(3):925-933.

34. Priya R, Dhanwani R, Patro IK, Rao PV, Parida MM. Differential regulation of TLR mediated innate immune response of mouse neuronal cells following infection with novel ECSA genotype of chikungunya virus with and without E1:A226V mutation. *Infect Genet Evol*. 2013;20:396-406.

35. Sharma A, Maheshwari RK. Oligonucleotide array analysis of toll-like receptors and associated signalling genes in venezuelan equine encephalitis virus-infected mouse brain. *J Gen Virol*. 2009;90(Pt 8):1836-1847.

36. Pasparakis M, Vandenabeele P. Necroptosis and its role in inflammation. *Nature*. 2015;517(7534):311-320.

37. Elmore S. Apoptosis: A review of programmed cell death. *Toxicol Pathol*. 2007;35(4):495-516.

38. Nava VE, Rosen A, Veliuona MA, Clem RJ, Levine B, Hardwick JM. Sindbis virus induces apoptosis through a caspase-dependent, CrmA-sensitive pathway. *J Virol*. 1998;72(1):452-459.

39. Irusta PM, Hardwick JM. Neuronal apoptosis pathways in sindbis virus encephalitis. *Prog Mol Subcell Biol*. 2004;36:71-93.

40. Nargi-Aizenman JL, Griffin DE. Sindbis virus-induced neuronal death is both necrotic and apoptotic and is ameliorated by N-methyl-D-aspartate receptor antagonists. *J Virol*. 2001;75(15):7114-7121.

41. Appel E, Katzoff A, Ben-Moshe T, et al. Differential regulation of bcl-2 and bax expression in cells infected with virulent and nonvirulent strains of sindbis virus. *Virology*. 2000;276(2):238-242.

42. Jackson AC, Moench TR, Griffin DE, Johnson RT. The pathogenesis of spinal cord involvement in the encephalomyelitis of mice caused by neuroadapted sindbis virus infection. *Lab Invest*. 1987;56(4):418-423.

43. Kerr DA, Larsen T, Cook SH, et al. BCL-2 and BAX protect adult mice from lethal sindbis virus infection but do not protect spinal cord motor neurons or prevent paralysis. *J Virol*. 2002;76(20):10393-10400.

44. Conrad M, Angeli JP, Vandenabeele P, Stockwell BR. Regulated necrosis: Disease relevance and therapeutic opportunities. *Nat Rev Drug Discov*. 2016;15(5):348-366.

45. Linkermann A, Stockwell BR, Krautwald S, Anders HJ. Regulated cell death and inflammation: An auto-amplification loop causes organ failure. *Nat Rev Immunol*. 2014;14(11):759-767.

46. Vanden Berghe T, Linkermann A, Jouan-Lanhouet S, Walczak H, Vandenabeele P. Regulated necrosis: The expanding network of non-apoptotic cell death pathways. *Nat Rev Mol Cell Biol*. 2014;15(2):135-147.

47. Huttmann J, Krause E, Schommartz T, Brune W. Functional comparison of molluscum contagiosum virus vFLIP MC159 with murine cytomegalovirus M36/vICA and M45/vIRA proteins. *J Virol*. 2015;90(6):2895-2905.

48. Schock SN, Chandra NV, Sun Y, et al. Induction of necroptotic cell death by viral activation of the RIG-I or STING pathway. *Cell Death Differ*. 2017.

49. Kaczmarek A, Vandenabeele P, Krysko DV. Necroptosis: The release of damage-associated molecular patterns and its physiological relevance. *Immunity*. 2013;38(2):209-223.

50. Pierdomenico M, Negroni A, Stronati L, et al. Necroptosis is active in children with inflammatory bowel disease and contributes to heighten intestinal inflammation. *Am J Gastroenterol*. 2014;109(2):279-287.

51. Zhao H, Jaffer T, Eguchi S, Wang Z, Linkermann A, Ma D. Role of necroptosis in the pathogenesis of solid organ injury. *Cell Death Dis*. 2015;6:e1975.

52. Liu S, Wang X, Li Y, et al. Necroptosis mediates TNF-induced toxicity of hippocampal neurons. *Biomed Res Int*. 2014;2014:290182.

53. Ito Y, Ofengeim D, Najafov A, et al. RIPK1 mediates axonal degeneration by promoting inflammation and necroptosis in ALS. *Science*. 2016;353(6299):603-608.

54. Re DB, Le Verche V, Yu C, et al. Necroptosis drives motor neuron death in models of both sporadic and familial ALS. *Neuron*. 2014;81(5):1001-1008.

55. Kanno H, Ozawa H, Tateda S, Yahata K, Itoi E. Upregulation of the receptor-interacting protein 3 expression and involvement in neural tissue damage after spinal cord injury in mice. *BMC Neurosci*. 2015;16:0.

56. Fan H, Zhang K, Shan L, et al. Reactive astrocytes undergo M1 microglia/macrohpages-induced necroptosis in spinal cord injury. *Mol Neurodegener*. 2016;11:8.

57. Schock SN, Chandra NV, Sun Y, et al. Induction of necroptotic cell death by viral activation of the RIG-I or STING pathway. *Cell Death Differ*. 2017.

58. Bian P, Zheng X, Wei L, et al. MLKL mediated necroptosis accelerates JEV-induced neuroinflammation in mice. *Front Microbiol*. 2017;8:303.

59. Berger AK, Hiller BE, Thete D, et al. Viral RNA at two stages of reovirus infection is required for the induction of necroptosis. *J Virol*. 2017;91(6):16. Print 2017 Mar 15.

60. Cho YS, Challa S, Moquin D, et al. Phosphorylation-driven assembly of the RIP1-RIP3 complex regulates programmed necrosis and virus-induced inflammation. *Cell*. 2009;137(6):1112-1123.

61. Huang Z, Wu SQ, Liang Y, et al. RIP1/RIP3 binding to HSV-1 ICP6 initiates necroptosis to restrict virus propagation in mice. *Cell Host Microbe*. 2015;17(2):229-242.

62. Thapa RJ, Ingram JP, Ragan KB, et al. DAI senses influenza A virus genomic RNA and activates RIPK3-dependent cell death. *Cell Host Microbe*. 2016;20(5):674-681.

63. Meessen-Pinard M, Le Coupanec A, Desforges M, Talbot PJ. Pivotal role of receptor-interacting protein kinase 1 and mixed lineage kinase domain-like in neuronal cell death induced by the human neuroinvasive coronavirus OC43. *J Virol*. 2016;91(1):16. Print 2017 Jan 1.

64. Kulcsar KA, Baxter VK, Abraham R, Nelson A, Griffin DE. Distinct immune responses in resistant and susceptible strains of mice during neurovirulent alphavirus encephalomyelitis. *J Virol*. 2015;89(16):8280-8291.

65. Carmen J, Rothstein JD, Kerr DA. Tumor necrosis factor-alpha modulates glutamate transport in the CNS and is a critical determinant of outcome from viral encephalomyelitis. *Brain Res*. 2009;1263:143-154.

66. Sarid R, Ben-Moshe T, Kazimirsky G, et al. vFLIP protects PC-12 cells from apoptosis induced by sindbis virus: Implications for the role of TNF-alpha. *Cell Death Differ*. 2001;8(12):1224-1231.

67. Wang Q, Yu M, Zhang K, et al. Expression profile and tissue-specific distribution of the receptor-interacting protein 3 in BALB/c mice. *Biochem Genet*. 2016;54(4):360-367.

68. Esen N, Blakely PK, Rainey-Barger EK, Irani DN. Complexity of the microglial activation pathways that drive innate host responses during lethal alphavirus encephalitis in mice. *ASN Neuro*. 2012;4(4):207-221.

69. Sethman CR, Hawiger J. The innate immunity adaptor SARM translocates to the nucleus to stabilize lamins and prevent DNA fragmentation in response to pro-apoptotic signaling. *PLoS One*. 2013;8(7):e70994.

70. Summers DW, Gibson DA, DiAntonio A, Milbrandt J. SARM1-specific motifs in the TIR domain enable NAD+ loss and regulate injury-induced SARM1 activation. *Proc Natl Acad Sci U S A*. 2016;113(41):E6280.

71. Guo YE, Steitz JA. Virus meets host microRNA: The destroyer, the booster, the hijacker. *Mol Cell Biol*. 2014;34(20):3780-3787.

72. Trobaugh DW, Klimstra WB. MicroRNA regulation of RNA virus replication and pathogenesis. *Trends Mol Med*. 2017;23(1):80-93.

73. Harrison EB, Hochfelder CG, Lamberty BG, et al. Traumatic brain injury increases levels of miR-21 in extracellular vesicles: Implications for neuroinflammation. *FEBS Open Bio*. 2016;6(8):835-846.

74. Alexander M, Hu R, Runtsch MC, et al. Exosome-delivered microRNAs modulate the inflammatory response to endotoxin. *Nat Commun*. 2015;6:7321.

75. Taganov KD, Boldin MP, Chang KJ, Baltimore D. NF-kappaB-dependent induction of microRNA miR-146, an inhibitor targeted to signaling proteins of innate immune responses. *Proc Natl Acad Sci U S A*. 2006;103(33):12481-12486.

76. He S, Huang S, Shen Z. Biomarkers for the detection of necroptosis. *Cell Mol Life Sci*. 2016;73(11-12):2177-2181.

77. Greene IP, Lee EY, Prow N, Ngwang B, Griffin DE. Protection from fatal viral encephalomyelitis: AMPA receptor antagonists have a direct effect on the inflammatory response to infection. *Proc Natl Acad Sci U S A*. 2008;105(9):3575-3580.

78. Darman J, Backovic S, Dike S, et al. Viral-induced spinal motor neuron death is non-cell-autonomous and involves glutamate excitotoxicity. *J Neurosci*. 2004;24(34):7566-7575.

79. Wegner KW, Saleh D, Degterev A. Complex pathologic roles of RIPK1 and RIPK3: Moving beyond necroptosis. *Trends Pharmacol Sci*. 2017;38(3):202-225.

80. Daniels BP, Snyder AG, Olsen TM, Orozco S, Oguin TH,3rd, Tait SW, Martinez J, Gale M,Jr, Loo YM, Oberst A. RIPK3 restricts viral pathogenesis via cell death-independent neuroinflammation. Cell 2017 Apr 6;169(2):301,313.e11.

81. Hambright WS, Fonseca RS, Chen L, Na R, Ran Q. Ablation of ferroptosis regulator glutathione peroxidase 4 in forebrain neurons promotes cognitive impairment and neurodegeneration. *Redox Biol*. 2017;12:8-17.

82. Blakely PK, Huber AK, Irani DN. Type-1 angiotensin receptor signaling in central nervous system myeloid cells is pathogenic during fatal alphavirus encephalitis in mice. *J Neuroinflammation*. 2016;13(1):7.

Kuo Gai

Address: 116 W. University Pkwy Apt 705, Baltimore, MD 21210
Mobile Phone: (410) 209-9798
Email: gaik22891218@gmail.com | kgai1@jhu.edu

EDUCATION

2015 - 2017	**Johns Hopkins Bloomberg School of Public Health**, ScM. Major: Molecular Microbiology and Immunology Advisor: Prof. Diane Griffin.
2011 - 2015	**The Chinese University of Hong Kong**, B.sc Major: Cell and Molecular Biology

RESEARCH EXPERIENCE

January 2014 - Present	**Graduate Student**, Johns Hopkins Bloomberg School of Public Health Supervisor: Dr. Diane Griffin Molecular indicators for the severity of Sindbis virus-induced encephalomyelitis
September 2014 - May 2015	**Undergraduate Student**, The Chinese University of Hong Kong Supervisor: Dr. Chu Ka Hou Structural study of two hypoallergenic mutants of shrimp tropomyosin Met e I
June 2014 - August 2014	**Summer Research Intern**, University of California, Davis Supervisor: Dr. Patrick SC Leung Tropomyosin specific monoclonal antibody production using hybridoma techniques

HONORS AND AWARDS

2014	**Dr. Tien Chang Lin Technology Innovation Foundation Scholarships**
2014	**Mr. Wu Sai Wing Memorial Scholarships**
2012	**Dean's List**
2011	**Mr. & Mrs. Chan Foo Chuen Scholarships**